Beamspace ML Bearing Estimation Incorporating Low-Angle Geometry

MICHAEL D. ZOLTOWSKI, Member, IEEE
Purdue University

TA-SUNG LEE, Student, IEEE
National Chiao Tung University

A problem of interest in low-angle radar tracking is that of bearing estimation in the presence of a strong specular multipath component that arrives within a beamwidth of the direct path signal. Three-dimensional beamspace domain maximum likelihood (3D-BDML) is a computationally simple ML bearing estimation algorithm applicable in this scenario which operates in a 3-D beamspace. A variation of 3D-BDML incorporating the multipath geometry as a priori information is presented. In symmetric 3D-BDML the pointing angle of the center beam is equal to the bisector angle between the direct path ray and the image ray, which may be estimated a priori given only the radar height and the target range. The effect of the inclusion of a priori information on the performance of 3D-BDML is analyzed in terms of the dependence on the relative phase difference between the direct and specular path signals, the sensitivity to error in the bisector angle estimate, and the results of operation when no specular multipath component is present in the data. In addition, computationally simple schemes for coherently incorporating multifrequency data into 3D-BDML are investigated as well.

Manuscript received November 21, 1989; revised May 25, 1990.

IEEE Log No. 44357.

This work was supported in part by the National Science Foundation under Grant ECS-8707681 and by the General Electric Company under Grant 1724670.

Authors' addresses: M. D. Zoltowski, School of Electrical Engineering, Purdue University, West Lafayette, IN 47907; T.-S. Lee, Dept. of Communication Engineering, National Chiao Tung University, Hsinchu, Taiwan, R.O.C.

I. INTRODUCTION

Low-angle radar tracking represents a classical problem in radar which has been attacked by numerous researchers for the past several decades [1–13]. The goal is to track a target flying at a low altitude, in relative terms, over a fairly smooth reflecting surface such as calm sea, for example. Echoes return to the radar site via a specular path as well as by a direct path. Due to the relatively small differential in length between the two paths, the direct and specular path signals arrive overlapped in time. In addition, the angular separation between the two ray paths is typically a fraction of a beamwidth. It is well known that the classical monopulse bearing estimation technique breaks down under these conditions. As a consequence, several alternative maximum likelihood (ML) based bearing estimation schemes have been proposed, each theoretically capable of resolving two targets separated by less than a beamwidth [2–13]. These various ML-based estimation schemes may be classified under two major categories: those which operate in element space and those which operate in beamspace. Pioneering work on the element space-based-ML estimator is attributed to Ksienski and McGhee [2]. The major drawback of the element space-based ML methods is the attendant computational complexity due to the required multidimensional search over a multimodal surface.

The bearing estimation technique employed in conventional monopulse radar may be interpreted as an ML estimator based in a 2-D beamspace defined by sum and difference beams [5]. As this technique is extremely computationally simple, a number of ML estimation schemes based in a suitably defined 3-D beamspace [6–9, 11–13] have been proposed for low-angle radar tracking. These may be classified into two categories. In the first category, the transformation from element space to 3-D beamspace is achieved by applying the same beamforming weight vector to each of three identical subarrays extracted from the overall array. The subarrays may or may not be overlapping. An example of this type of estimation scheme is the three-subaperture (3-APE) scheme of Cantrell, Gordon, and Trunk [6, 9]. In the second category, the prescription for converting to 3-D beamspace is to apply three different beamforming weight vectors to all of the array elements. Examples of this type of estimation scheme include the least squares adaptive antenna (LSAA) method of Kesler and Haykin [7–8] and the 3-D beamspace domain maximum likelihood (3D-BDML) method of Zoltowski and Lee [11–13]. Each of the these three methods, 3-APE, LSAA, and 3D-BDML, is computationally simplistic in deference to the need for real time applicability.

A novel and practical approach to low-angle radar tracking is described in the pioneering work of White

[3]. An important aspect of the method of White is that it incorporates a priori knowledge with regard to the multipath geometry. The premise is that if the surface is smooth enough to provide a specular reflection, then it is also predictable. Simple geometry yields the angle of the image ray corresponding to each direct path ray in terms of the height of the radar above the surface and the range of the target. Although the theoretical development of the bearing estimation procedure of White in [3] was presented in element space terms, the actual antenna utilized for tracking was not an array. Rather, it employed a cluster of six horns feeding a Cassegrain dual reflector antenna. The six horns were arranged in three pairs stacked in elevation, with each pair providing sum and difference beams in azimuth. One pair yielded beams above the boresight axis, another yielded beams pointed to elevation boresight, while the third pair provided beams below boresight. A combining network provided a sum beam and a normal elevation difference output. A second elevation difference pattern provided an output signal that varied as the square of the displacement from boresight. At high angles where multipath is not a problem, only the normal difference signal is used in forming the elevation error signal. At low angles, a calibrated portion of the second difference is used to generate a second null at the expected angle of the specular reflection. As a consequence of the exploitation of the multipath geometry, the search process even at low angles is only over one independent angle variable.

The performance of any bearing estimation scheme in a low-angle radar tracking scenario is dependent on the phase difference between the direct and specular path signals. As a consequence of the fraction of a beamwidth angular separation between the two ray paths, the phase difference between the two signals does not vary much across the array. Let $\Delta\Psi$ denote the phase difference between the direct and specular path signals at the center of the array. In addition to effectively reducing a two-dimensional (2-D) parameter estimation problem to a one-dimensional (1-D) one, the incorporation of the multipath geometry as a priori information also has a favorable effect with regard to the dependence on $\Delta\Psi$. Without the incorporation of such, the ML method in either element space or beamspace experiences large errors when $\Delta\Psi$ is either 0° or 180° [3, 6, 13]. With a priori information included, $\Delta\Psi = 0^\circ$ is no longer a problem and, in fact, yields best performance. The $\Delta\Psi = 180^\circ$ case still remains a problem, however. One obvious means for overcoming this problem is to employ frequency diversity.

Recently, Kezys and Haykin [18] describe an ML-based bearing estimation scheme for low-angle radar tracking which incorporates frequency diversity as well as a priori information with regard to the multipath geometry. A novel aspect of their method is that it explicitly accounts for some level of inaccuracy in the knowledge of both the radar height and the target range. However, the method is based in element space and is quite computationally burdensome involving a search with respect to ten parameters. The computational complexity is abated somewhat by the imposition of equality constraints which exploit the linear dependence of the relative phase difference between the direct and specular path signals with respect to frequency. It should also be pointed out that the method has been demonstrated to perform quite well with experimental (real) data for angular separations between the two signals as small as a quarter of a beamwidth.

As an alternative, we here present a variation of our earlier beamspace domain based method, 3D-BDML [11–13], which incorporates frequency diversity and a priori information in the form of the bisector angle between the direct path ray and the image ray. This may be estimated given only the height of the radar array and the range of the target as shown in Section II. In Section III, symmetric 3D-BDML is formulated by setting the pointing angle of the center of three orthogonal beams, equi-spaced in elevation, equal to the bisector angle. It is shown that, in effect, symmetric 3D-BDML exploits the underlying symmetry by preprocessing in the form of a forward-backward average of the 3×3 beamspace correlation matrix formed from the three respective beam outputs. An ML bearing estimator operating in a 2-D beamspace is also developed in Section III as a simplification of 3D-BDML for high angles in which multipath is not a problem. In Section IV, the effects of the forward-backward average in beamspace are analyzed in terms of the dependence of symmetric 3D-BDML on $\Delta\Psi$, the performance of symmetric 3D-BDML when no specular multipath component is present, and the degradation in performance incurred in symmetric 3D-BDML with estimation error in the bisector angle. A multifrequency version of symmetric 3D-BDML is developed in Section V. The coherent signal subspace concept of Wang and Kaveh [11, 12] is invoked as a means for retaining the computational simplicity of 3-D BDML in the case of single frequency operation, while incorporating in a coherent manner the additional data obtained at the auxiliary frequencies. Finally, simulations are presented in Section VI as a means of validating results derived throughout.

II. BISECTOR ANGLE DETERMINATION FROM MULTIPATH GEOMETRY

Consider the geometry of the low-angle radar tracking scenario in the case of a flat Earth model as depicted in Fig. 1. A target is flying at a relatively low altitude over the sea surface. The variable R_t denotes the range of the target, h_r denotes the height of the

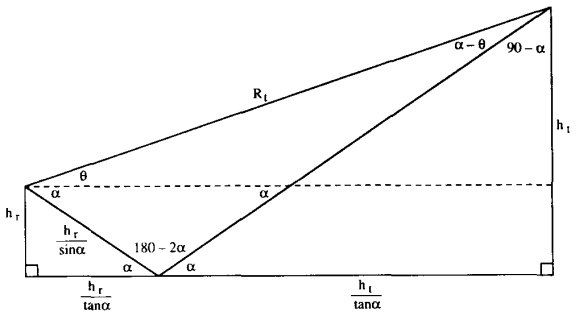

Fig. 1. Multipath geometry for low-angle radar tracking scenario for case of flat Earth model.

center of the receiving array above sea level, and h_t denotes the height of the target above sea level, i. e., the target altitude. Echoes return to the radar site via a specular path as well as by a direct path. θ is the angle of the direct path ray measured upward with respect to broadside to the array, while α is the angle of the specular path ray measured downward from broadside to the array. In this notation, the bisector angle is $\theta_B = (\theta - \alpha)/2$. The other angles indicated in Fig. 1 were determined from α and θ in accordance with Snell's law of reflection and the fact that the sum of the angles in a triangle is 180°. Invoking the law of sines, $\theta_B = (\theta - \alpha)/2$ may be approximated, to a high degree of precision, with only knowledge of h_r and R_t. The appropriate development is as follows.

The law of sines dictates

$$\frac{h_r/\sin\alpha}{\sin(\alpha-\theta)} = \frac{R_t}{\sin(180-2\alpha)}. \tag{1}$$

Substitution of the trigonometric identity $\sin(180 - 2\alpha) = \sin(2\alpha) = 2\sin\alpha\cos\alpha$ coupled with simple algebraic manipulation yields

$$\sin(\alpha-\theta) = 2\frac{h_r}{R_t}\cos\alpha. \tag{2}$$

In the low-angle radar scenario, α is rather small such that $\cos\alpha \approx 1$. Incorporating this approximation yields

$$\theta_B = \frac{\theta-\alpha}{2} \approx -\frac{1}{2}\sin^{-1}\left\{2\frac{h_r}{R_t}\right\}. \tag{3}$$

Finally, invoking the fact that $h_r/R_t \ll 1$ in the $u = \sin(\theta)$ domain yields

$$u_B \approx -\frac{h_r}{R_t} \tag{4}$$

where $u_B = \frac{1}{2}\{\sin\theta - \sin\alpha\}$. In the case of a flat-Earth model, this is the estimate of the bisector angle to be employed by the symmetric 3D-BDML bearing estimator developed in Section III.

Now, R_t is only known to within a certain tolerance based on the dimensions of range bin in which the target is located. Let ΔR_t be the error in the range estimate. For the practical case where $\Delta R_t \ll R_t$

$$\frac{h_r}{R_t+\Delta R_t} = \frac{h_r}{R_t}\left\{\frac{1}{1+\Delta R_t/R_t}\right\} \approx \frac{h_r}{R_t}\left\{1-\frac{\Delta R_t}{R_t}\right\} = \frac{h_r}{R_t} - \frac{\Delta R_t}{R_t^2}. \tag{5}$$

Thus, the additive "bias" in the bisector angle estimate due to inaccurate knowledge of the target range is inversely proportional to the square of the target range!! Notwithstanding, the effect of an error in the bisector angle estimate on the performance of symmetric 3D-BDML is examined in Section IV.

The expression for the bisector angle in (4) is approximately equal to the angle of a ray from the center of the array to a point on the surface directly under the target. This observation provides the motivation for a method of approximating the bisector angle in long range applications where the curvature of the Earth must be taken into account. Approximating the Earth as a sphere with known radius, consider a plane that is tangent to the surface at the reflection point. To a high degree of precision, the bisector angle may be approximated as the angle of a ray from the center of the array to a point on this tangent plane directly below the target. Now, the location of the tangent point depends on the target height such that, in the case of a spherical Earth model, the bisector angle depends on the target height in addition to the radar height and the target range. Fortunately, however, the dependence is not great as demonstrated in Table I. Table I lists the values of the angle of the direct path ray, the angle of the image ray, and the bisector angle as a function of target height for a target range of 5 nmi and a radar height of 60 ft. Refraction effects were accounted for by using a radius equal to 4/3 times the true radius of the Earth. It is observed that as the target height varies from 0 to 200 ft, the bisector angle only varies by roughly plus or minus one hundredth of a degree from the value computed for a target height equal to the radar height of 60 ft. Thus, in the case of a spherical Earth model, the bisector angle estimate to be used in symmetric 3D-BDML is the angle from the array center to a point directly under the target on the plane tangent to the surface of the Earth at the point of reflection, computed for a target height equal to the radar height. Again, the effect of an error in the bisector angle estimate on the performance of symmetric 3D-BDML is examined in Section IV.

III. 3-D BEAMSPACE ML BEARING ESTIMATION FOR TWO-RAY MULTIPATH

We here present a brief development of the 3D-BDML bearing estimator for low-angle radar tracking. The reader is referred to [13, 22] for a more detailed development. As a means for differentiating

TABLE I
Bisector Angle Estimates with Spherical Earth Model Target Range: 5 nmi; Radar Height: 60 ft

Target Ht Feet	Elevation Angle in degrees Direct Path	Image Path	Bisector Angle
10	−0.1240	−0.1604	−0.1422
20	−0.1053	−0.1768	−0.1411
30	−0.0869	−0.1931	−0.1400
40	−0.0684	−0.2093	−0.1389
50	−0.0499	−0.2256	−0.1377
60	−0.0312	−0.2419	−0.1366
80	0.0062	−0.2752	−0.1345
100	0.0438	−0.3090	−0.1326
120	0.0815	−0.3434	−0.1310
140	0.1192	−0.3783	−0.1296
160	0.1569	−0.4136	−0.1283
180	0.1946	−0.4491	−0.1273
200	0.2324	−0.4850	−0.1263
250	0.3268	−0.5756	−0.1244
300	0.4211	−0.6671	−0.1230
400	0.5979	−0.8395	−0.1208
500	0.7859	−1.0249	−0.1195

among the various BDML estimators to be developed within, the estimation scheme presented in [13] is here referred to as nonsymmetric 3D-BDML. The development of nonsymmetric 3D-BDML is then simply modified to incorporate a priori information with regard to the bisector angle yielding an estimation scheme referred to as symmetric 3D-BDML. Finally, a 2-D beamspace domain ML estimator (2D-BDML) is derived from the nonsymmetric 3D-BDML estimator for use in cases in which the specular multipath component is either nil or negligible. It should be noted that symmetric 3D-BDML works properly, i.e., provides accurate estimates of the target bearing angle, even in rough sea surface scenarios where there is no measurable specular multipath component at the receiving array. This assertion is justified analytically in Section III and is backed up by simulation results presented in Section VI.

A. Array Data Model

The data for the 3D-BDML estimator is the collection of signals received at a radar antenna array. It is here assumed that the array is linear and composed of M elements uniformly spaced by half the wavelength of the transmitted pulse. It is further assumed that the array is mounted vertically to monitor target elevation. Due to the low elevation angle of target, assumed to be in the far-field, the direct and specular path signals arrive overlapping in time and angularly separated by less than the nominal 3 dB beamwidth at broadside. In the case of a uniformly spaced linear array (ULA) of M elements, the nominal 3 dB beamwidth at broadside is approximately $2/M$. Let $\mathbf{x}(n)$ denote the $M \times 1$ snapshot vector. The ith element of $\mathbf{x}(n)$ is $x_i(n)$, $i = 1,\ldots,M$, the value of the complex analytic signal outputted from the ith element of the array measured at discrete time n. Invoking the standard narrowband model, $\mathbf{x}(n)$ may be expressed as

$$\begin{aligned}\mathbf{x}(n) &= c_1(n)\mathbf{a}_M(u_1) + c_2(n)\mathbf{a}_M(u_2) \\ &\quad + \mathbf{n}(n) \qquad n = 1,\ldots,N \\ &= \left[\mathbf{a}_M(u_1) : \mathbf{a}_M(u_2)\right]\begin{bmatrix} c_1(n) \\ c_2(n)\end{bmatrix} + \mathbf{n}(n) \\ &= \mathbf{A}\mathbf{c}(n) + \mathbf{n}(n) \end{aligned} \tag{6}$$

where $c_1(n)$ is the sample value of the complex envelope of the direct path echo at the nth snapshot and $u_1 = \sin\theta_1$; θ_1 denotes the arrival angle of the direct path signal. $c_2(n)$ and θ_2 are defined similarly with respect to the specular path signal. In terms of the notation in Fig. 1, $\theta_1 = \theta$ and $\theta_2 = -\alpha$. The elements of $\mathbf{n}(n)$ constitute the complex noise present at each antenna output at the nth snapshot.

The phase angle of $c_1(n)$ is that measured at the center of the array such that $\mathbf{a}_M(u_1)$ accounts for a linear phase variation across the array due the planar nature of the wavefront arriving via the direct path. Similar comments hold with regard to role of $\mathbf{a}_M(u_2)$ in the case of the specular path signal. For the case of M odd such that $M = 2K + 1$, where K is an integer,

$$\begin{aligned}\mathbf{a}_M(u) = [&e^{-j\pi Ku},\ldots,e^{-2j\pi u},e^{-j\pi u},1, \\ &e^{j\pi u},e^{2j\pi u},\ldots,e^{j\pi Ku}]^T \qquad \text{if} \quad M = 2K+1.\end{aligned} \tag{7a}$$

On the other hand, for M even such that $M = 2K$, where K is an integer,

$$\begin{aligned}\mathbf{a}_M(u) = [&e^{-j\pi(K-(1/2))u},\ldots,e^{-j\pi(3/2)u},e^{-j\pi(u/2)}, \\ &e^{j\pi(u/2)},e^{j\pi(3/2)u},\ldots,e^{j\pi(K-(1/2))u}]^T \\ &\text{if} \quad M = 2K.\end{aligned} \tag{7b}$$

The subscript M on either of these entities is intended to designate the dimension of the vector $\mathbf{a}_M(u)$. We note that when $\mathbf{a}_M(u)$ for some specific value of u is employed as a weight vector applied to $\mathbf{x}(n)$, the operation is referred to as classical beamforming.

In the 3D-BDML scheme, a 3×1 beamspace snapshot vector, denoted $\mathbf{x}_B(n)$, is formed as

$$\mathbf{x}_B(n) = \mathbf{S}_M^H\mathbf{x}(n) \tag{8}$$

where $\mathbf{S}_M$ is the $M \times 3$ matrix beamformer

$$\mathbf{S}_M = \frac{1}{\sqrt{M}}\left[\mathbf{a}_M\left(u_c - \frac{2}{M}\right) : \mathbf{a}_M(u_c) : \mathbf{a}_M\left(u_c + \frac{2}{M}\right)\right] \tag{9}$$

with $\mathbf{a}_M(u)$ defined previously in (7). The $M \times 3$ beamforming matrix $\mathbf{S}_M$ serves to form a center beam pointed to u_c, and two beams pointed symmetrically above and below u_c at $u = u_c + 2/M$ and $u = u_c -$

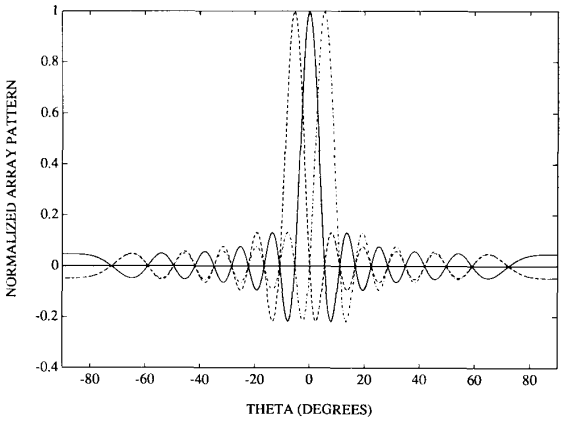

Fig. 2. Plot of normalized array patterns associated with each of three mutually orthogonal, classical beamformers with pointing angles of $-5.46°$, $0°$, and $5.46°$, respectively, for case of $M = 21$ element array uniformly spaced by a half-wavelength. Array patterns have $M - 3 = 18$ nulls in common.

$2/M$, respectively. The three respective beam patterns for the case of $u_c = 0$ and $M = 21$ are depicted in Fig. 2. It is observed that each beam has a null in the location of the peak of the respective mainlobe associated with each of the other two beams. This is a consequence of the fact that the columns of $\mathbf{S}_M$ are mutually orthogonal, i.e., $\mathbf{S}_M^H \mathbf{S}_M = \mathbf{I}_3$.

Substituting (6) into (8) and defining $\mathbf{b}(u) = \mathbf{S}_M^H \mathbf{a}_M(u)$ as the 3×1 beamspace manifold vector yields

$$\mathbf{x}_B(n) = \left[\mathbf{b}(u_1) \vdots \mathbf{b}(u_2)\right] \mathbf{c}(n) + \mathbf{S}_M^H \mathbf{n}(n) = \mathbf{B}\mathbf{c}(n) + \mathbf{n}_B(n) \tag{10}$$

where $\mathbf{B} = [\mathbf{S}_M^H \mathbf{a}_M(u_1) \vdots \mathbf{S}_M^H \mathbf{a}_M(u_2)] = [\mathbf{b}(u_1) \vdots \mathbf{b}(u_2)]$ and $\mathbf{n}_B(n) = \mathbf{S}_M^H \mathbf{n}(n)$. Let us examine the structure of the 3×1 beamspace manifold vector $\mathbf{b}(u) = \mathbf{S}_M^H \mathbf{a}_M(u)$. Invocation of the definitions of $\mathbf{a}_M(u)$ and $\mathbf{S}_M$ in (9) and (7), respectively, yields a component-wise expression for $\mathbf{b}(u)$:

$$\mathbf{b}(u) = \left[\frac{\sin\left(M\frac{\pi}{2}\left(u - u_c + \frac{2}{M}\right)\right)}{\sin\left(\frac{\pi}{2}\left(u - u_c + \frac{2}{M}\right)\right)}, \frac{\sin\left(M\frac{\pi}{2}(u - u_c)\right)}{\sin\left(\frac{\pi}{2}(u - u_c)\right)}, \frac{\sin\left(M\frac{\pi}{2}\left(u - u_c - \frac{2}{M}\right)\right)}{\sin\left(\frac{\pi}{2}\left(u - u_c - \frac{2}{M}\right)\right)} \right]^T. \tag{11}$$

Note that $\mathbf{b}(u)$ is real-valued for all u. This property is a consequence of the conjugate centrosymmetry of $\mathbf{a}_M(u)$ defined in (7) and is invoked in both the nonsymmetric and symmetric versions of 3D-BDML to be presented shortly. An additional property of $\mathbf{b}(u)$ critical in the development and analysis of the symmetric 3D-BDML estimator is

$$\tilde{\mathbf{I}}_3 \mathbf{b}(u) = \mathbf{b}(2u_c - u) \quad \text{or} \quad \tilde{\mathbf{I}}_3 \mathbf{b}(u_c + \Delta) = \mathbf{b}(u_c - \Delta) \tag{12}$$

where $\tilde{\mathbf{I}}_3$ is the 3×3 reverse permutation matrix

$$\tilde{\mathbf{I}}_3 = \begin{bmatrix} 0 & 0 & 1 \\ 0 & 1 & 0 \\ 1 & 0 & 0 \end{bmatrix}. \tag{13}$$

The property in (12) is easily verified by invoking the fact that

$$\frac{\sin\left(M\frac{\pi}{2}u\right)}{\sin\left(\frac{\pi}{2}u\right)}$$

is an even function of u. Note that $\tilde{\mathbf{I}}_3$ in (13) satisfies $\tilde{\mathbf{I}}_3^T = \tilde{\mathbf{I}}_3$ and $\tilde{\mathbf{I}}_3 \tilde{\mathbf{I}}_3 = \mathbf{I}_3$. These properties of $\tilde{\mathbf{I}}_3$ are exploited in the development and analysis of symmetric 3D-BDML.

B. Nonsymmetric 3D-BDML Bearing Estimator

Assuming the receiver generated noise at each of the M antenna elements to be independent and identically distributed (IID), the Central Limit Theorem may be invoked in the practical case of M large to adequately model $\mathbf{n}_B(n)$ as a 3x1 multivariate Gaussian distributed random vector with zero mean. Recall that the columns of $\mathbf{S}_M$ are orthogonal. If the expected power of the noise at each element is of nearly equal power, it is also adequate to model the components of $\mathbf{n}_B(n)$ to be independent and of equal power. As a consequence of these observations, the 3D-BDML estimates of u_1 and u_2 may be formulated as the solution to the following nonlinear least squares problem

$$\underset{u_1,u_2,\mathbf{c}(1),\ldots,\mathbf{c}(N)}{\text{Minimize}} \sum_{n=1}^{N} \|\mathbf{x}_B(n) - \mathbf{B}(u_1,u_2)\mathbf{c}(n)\|^2 \tag{14}$$

where N is the number of snapshots. For the sake of generality, we consider the general case of multiple snapshots, although in practice the procedure may be limited to working with a single snapshot as in the simulations are presented in Section VI. Assuming the signals $c_1(n)$ and $c_2(n)$ to be unknown but deterministic, we invoke separability and substitute in (14) the respective least square error solution $\mathbf{c}_{LS}(n) = [\mathbf{B}^T\mathbf{B}]^{-1}\mathbf{B}^T\mathbf{x}_B(n)$, $n = 1,\ldots,N$. This yields

$$\underset{u_1,u_2}{\text{Minimize}} \sum_{n=1}^{N} \mathbf{x}_B^H(n)\mathbf{P}_B^{\perp}(u_1,u_2)\mathbf{x}_B(n) \tag{15}$$

where $\mathbf{P}_B^{\perp}(u_1,u_2) = \mathbf{I}_3 - \mathbf{B}[\mathbf{B}^T\mathbf{B}]^{-1}\mathbf{B}^T$. $\mathbf{P}_B^{\perp}(u_1,u_2)$ is a projection operator onto the 1-D space orthogonal

to the span of $\mathbf{b}(u_1)$ and $\mathbf{b}(u_2)$. Hence, $\mathbf{P}_B^{\perp}(u_1,u_2) = \mathbf{v}\mathbf{v}^T/\mathbf{v}^T\mathbf{v}$, where $\mathbf{v}$ satisfies

$$\mathbf{v}^T\mathbf{b}(u_i) = 0, \qquad i = 1,2. \tag{16}$$

Since $\mathbf{b}(u_1)$ and $\mathbf{b}(u_2)$ are both real-valued, $\mathbf{v}$ must be real-valued to within a complex-valued scalar multiple. Without loss of generality, we take $\mathbf{v}$ to be real-valued. At this point, we convert the search over u_1 and u_2 to a search over $\mathbf{v}$ by substituting $\mathbf{P}_B^{\perp}(u_1,u_2) = \mathbf{v}\mathbf{v}^T/\mathbf{v}^T\mathbf{v}$ in (15). This yields

$$\underset{\mathbf{v}}{\text{Minimize}} \frac{\sum_{n=1}^{N}\mathbf{x}_B^H(n)\mathbf{v}\mathbf{v}^T\mathbf{x}_B(n)}{\mathbf{v}^T\mathbf{v}} = N\frac{\mathbf{v}^T\text{Re}\{\hat{\mathbf{R}}_{bb}\}\mathbf{v}}{\mathbf{v}^T\mathbf{v}} \tag{17}$$

where $\hat{\mathbf{R}}_{bb}$ is the 3×3 beamspace domain sample correlation matrix

$$\hat{\mathbf{R}}_{bb} = \frac{1}{N}\sum_{n=1}^{N}\mathbf{x}_B(n)\mathbf{x}_B^H(n). \tag{18}$$

The solution for $\mathbf{v}$ in (17) is that eigenvector of $\text{Re}\{\hat{\mathbf{R}}_{bb}\}$ associated with the smallest eigenvalue. Given this $\mathbf{v}$, the 3D-BDML estimates of u_1 and u_2 are found via the relationship in (16). We expand on this final point.

Substituting $\mathbf{v} = [v_1, v_2, v_3]^T$ and $\mathbf{b}(u_i) = \mathbf{S}_M^H\mathbf{a}(u_i)$ into (16) and expanding yields

$$\begin{aligned}\mathbf{v}^T\mathbf{S}_M^H\mathbf{a}_M(u_i) &= v_1\mathbf{a}_M^H\left(u_c - \frac{2}{M}\right)\mathbf{a}_M(u_i) + v_2\mathbf{a}_M^H(u_c)\mathbf{a}_M(u_i) \\ &\quad + v_3\mathbf{a}_M^H\left(u_c + \frac{2}{M}\right)\mathbf{a}_M(u_i) = 0, \qquad i = 1,2.\end{aligned} \tag{19}$$

Without loss of generality, consider the case of M odd such that $M = 2K + 1$. Factoring $e^{-j\pi Ku_i}$ out of (19) yields

$$\begin{aligned}e^{-j\pi Ku_i}\Bigg(v_1\mathbf{a}_M^H\left(u_c - \frac{2}{M}\right)\mathbf{z}_M(z_i) + v_2\mathbf{a}_M^H(u_c)\mathbf{z}_M(z_i) \\ + v_3\mathbf{a}_M^H\left(u_c + \frac{2}{M}\right)\mathbf{z}_M(z_i)\Bigg) = 0, \qquad i = 1,2\end{aligned} \tag{20}$$

where

$$\begin{aligned}&\mathbf{z}_M(z_i) = [1, z_i, z_i^2, z_i^3, \ldots, z_i^{M-1}]^T \\ &\text{with} \quad z_i = e^{j\pi u_i}, \qquad i = 1,2.\end{aligned} \tag{21}$$

Denoting $\mathbf{S}_M\mathbf{v} = [w_0, w_1, \ldots, w_{M-1}]^H$, it follows from these observations that $z_i = e^{j\pi u_i}$, $i = 1,2$ are two of the $M-1$ roots of the polynomial

$$w(z) + w_0 + w_1 z + w_2 z^2 + \cdots + w_{M-1}z^{M-1} = 0. \tag{22}$$

To simplify further, note that the respective three beams associated with each of the columns of $\mathbf{S}_M$ defined in (9) have $M-3$ nulls in common. This phenomenon is depicted in Fig. 2 for the case of $M = 21$ wherein we observe $M - 3 = 18$ nulls in common among the three beams. This commonality of nulls translates into a condition that each of the three polynomials formed with a particular column of $\mathbf{S}_M$ as the corresponding coefficients has $M-3$ roots in common with the other two polynomials. It is easily shown [13, 22] that the $M-3$ common roots are located on the unit circle at $z_m = e^{j\pi(u_c+2m/M)}$, $m = 2,\ldots,M-2$. Observing (20) and (21), we note that $w(z)$ in (22) is simply a linear combination of the three polynomials constructed from the columns of $\mathbf{S}_M$. Thus, the two roots of $w(z)$ in (22) of interest are those of a quadratic equation obtained via the polynomial division

$$q(z) = q_0 + q_1 z + q_2 z^2 = \frac{w(z)}{\prod_{m=2}^{M-2}\left(z - e^{j\pi(u_c+2m/M)}\right)}. \tag{23}$$

This polynomial division may be accomplished via simple algebraic manipulation to yield expressions for the coefficients of $q(z)$ in terms of the components of $\mathbf{v}$ and M, the number of elements. The resulting expressions are

$$\begin{aligned}q_0 &= e^{j\pi u_c}\left\{-v_1e^{j(\pi/M)} + v_2 - v_3e^{-j(\pi/M)}\right\} = q_2^*; \\ q_1 &= 2(v_1 + v_3)\cos\left(\frac{\pi}{M}\right) - 2v_2\cos\left(\frac{2\pi}{M}\right).\end{aligned} \tag{24}$$

A summary of nonsymmetric 3D-BDML is then as follows. Compute $\mathbf{v} = [v_1, v_2, v_3]^T$ as that eigenvector of $\text{Re}\{\hat{\mathbf{R}}_{bb}\}$ associated with the smallest eigenvalue. Form the coefficients of the quadratic equation $q(z)$ according to the expressions in (24). Compute z_1 and z_2 as the two roots of $q(z)$. The 3D-BDML estimates of u_1 and u_2 are $\hat{u}_1 = (1/j\pi)\ln\{z_1\}$ and $\hat{u}_2 = (1/j\pi)\ln\{z_2\}$.

It is noted that nonsymmetric 3D-BDML is very similar to the beamspace version of MUSIC [17] for the case of two signals and operation in a beamspace of dimension three. The primary difference between the two is the fact that nonsymmetric 3D-BDML computes the so-called noise eigenvector [17] as the "smallest" eigenvector of the real part of $\hat{\mathbf{R}}_{bb}$ while MUSIC computes such as the smallest eigenvector of $\hat{\mathbf{R}}_{bb}$ itself. Here smallest eigenvector refers to that eigenvector associated with the smallest eigenvalue. This has implications with regard to performance in the case of a single snapshot and/or fully correlated signals. It is well known that MUSIC, stripped of spatial smoothing [15] and/or forward-backward averaging [16], breaks down under these conditions. On the other hand, as shown in Section IV nonsymmetric 3D-BDML is able to handle fully correlated signals as long as the relative phase difference between the two, $\Delta\Psi$, is neither 0° or 180°.

It should be noted that MUSIC is not an ML-based estimation scheme.

C. Symmetric 3D-BDML Bearing Estimator

The development of nonsymmetric 3D-BDML is easily modified to incorporate an a priori estimate of the bisector angle $u_B = (u_1 + u_2)/2$. With $u_c = u_B = (u_1 + u_2)/2$ in (11), invocation of the property of $\mathbf{b}(u)$ in (12) yields the following relationship between $\mathbf{b}(u_1)$ and $\mathbf{b}(u_2)$

$$\mathbf{b}(u_2) = \tilde{\mathbf{I}}_3\mathbf{b}(u_1) \tag{25}$$

where $\tilde{\mathbf{I}}_3$ is the 3×3 reverse permutation matrix defined previously in (13). The translation of (16) for the case of $u_c = u_B = (u_1 + u_2)/2$ yields the following pair of relationships between $\mathbf{v}$ and u_1:

$$\mathbf{v}^T\mathbf{b}(u_1) = 0 \qquad \text{and} \qquad \mathbf{v}^T\tilde{\mathbf{I}}_3\mathbf{b}(u_1) = 0. \tag{26}$$

These relationships imply that $\mathbf{v}$ must satisfy $\tilde{\mathbf{I}}_3\mathbf{v} = \mathbf{v}$, i.e., $\mathbf{v}$ must exhibit centro-symmetry. Hence, the condition $u_c = u_B$ dictates the incorporation of the constraint $\tilde{\mathbf{I}}_3\mathbf{v} = \mathbf{v}$ into the optimization problem described by (17).

$$\begin{aligned} &\underset{\mathbf{v}}{\text{Minimize}} \quad \frac{\mathbf{v}^T \text{Re}\{\hat{\mathbf{R}}_{bb}\}\mathbf{v}}{\mathbf{v}^T\mathbf{v}} \\ &\text{subject to:} \quad \tilde{\mathbf{I}}_3\mathbf{v} = \mathbf{v}. \end{aligned} \tag{27}$$

Since $\mathbf{v}$ is constrained to be centro-symmetric, we may express the objective function in (27) in an alternative fashion as:

$$\begin{aligned} &\underset{\mathbf{v}}{\text{Minimize}} \quad \frac{\frac{1}{2}\mathbf{v}^T[\text{Re}\{\hat{\mathbf{R}}_{bb}\} + \tilde{\mathbf{I}}_3\text{Re}\{\hat{\mathbf{R}}_{bb}\}\tilde{\mathbf{I}}_3]\mathbf{v}}{\frac{1}{2}\mathbf{v}^T[\mathbf{I} + \tilde{\mathbf{I}}_3\tilde{\mathbf{I}}_3]\mathbf{v}} \\ &\qquad\qquad = \frac{\mathbf{v}^T \text{Re}\{\hat{\mathbf{R}}_{bb}^{fb}\}\mathbf{v}}{\mathbf{v}^T\mathbf{v}} \\ &\text{subject to:} \quad \tilde{\mathbf{I}}_3\mathbf{v} = \mathbf{v} \end{aligned} \tag{28}$$

where

$$\hat{\mathbf{R}}_{bb}^{fb} = \tfrac{1}{2}\{\hat{\mathbf{R}}_{bb} + \tilde{\mathbf{I}}_3\hat{\mathbf{R}}_{bb}\tilde{\mathbf{I}}_3\} \tag{29}$$

may be interpreted as a forward-backward averaged beamspace sample correlation matrix [16]. It can be shown [22] that two of the eigenvectors of $\text{Re}\{\hat{\mathbf{R}}_{bb}^{fb}\}$ exhibit centro-symmetry while the third exhibits centro-antisymmetry. Thus, the minimizing $\mathbf{v}$ in (28) is that centro-symmetric eigenvector of $\text{Re}\{\hat{\mathbf{R}}_{bb}^{fb}\}$ associated with the smaller eigenvalue.

Given $\mathbf{v} = [v_1, v_2, v_1]^T$ obtained from this procedure, we may proceed to find the symmetric 3D-BDML estimate of u_1 using the same approach as in nonsymmetric 3D-BDML. The variable $z_1 = e^{j\pi u_1}$ and $z_2 = e^{j\pi u_2}$ are found as the two roots of $q(z)$ determined via a polynomial division of the form in (23) with $v_3 = v_1$. Consequently, the coefficients of $q(z)$ are given by (24) with $v_3 = v_1$:

$$\begin{aligned} q_0 &= e^{j\pi u_c}\left\{v_2 - 2v_1\cos\left(\frac{\pi}{M}\right)\right\} = q_2^*; \\ q_1 &= 4v_1\cos\left(\frac{\pi}{M}\right) - 2v_2\cos\left(\frac{2\pi}{M}\right). \end{aligned} \tag{30}$$

It is easily shown that if $|q_1/q_0| < 2$, the roots of $q(z)$ lie on the unit circle and may be expressed in terms of q_1 and q_0 as

$$\begin{aligned} z_{1,2} &= \frac{-q_1 \pm \sqrt{q_1^2 - 4|q_0|^2}}{2q_0} \\ &= e^{j\pi u_c}\left\{\frac{-q_1 \pm j\sqrt{4q_{0_r} - q_1^2}}{2q_{0_r}}\right\} \end{aligned} \tag{31}$$

where $q_{0_r} = v_2 - 2v_1\cos(\pi/M)$. If $|q_1/q_0| > 2$, the two roots of $q(z)$ have the same phase angle, πu_c, with the magnitude of one equal to the reciprocal of the other; this is an indication that the direct and specular path signals have not been resolved. If $|q_1/q_0| < 2$, the quantity in brackets in the far right-hand side (RHS) of (31) lies on the unit circle such that the two roots lie on the unit circle and are equi-distant from the point $z = e^{j\pi u_c}$. Equating the phase angle of the far RHS of (31) with that of $z_1 = e^{j\pi u_1}$ yields, after some algebraic manipulation, an expression for $\hat{u}_1$ in terms of M and the components of $\mathbf{v} = [v_1, v_2, v_1]^T$, the centro-symmetric eigenvector of $\text{Re}\{\hat{\mathbf{R}}_{bb}^{fb}\}$ defined by (29) associated with the smaller eigenvalue:

$$\hat{u}_1 = u_c + \frac{1}{\pi}\tan^{-1}\left\{\sqrt{\left\{\frac{v_2 - 2v_1\cos\left(\frac{\pi}{M}\right)}{v_2\cos\left(\frac{2\pi}{M}\right) - 2v_1\cos\left(\frac{\pi}{M}\right)}\right\}^2 - 1}\right\}. \tag{32}$$

D. 2D-BDML Bearing Estimator

The development of nonsymmetric 3D-BDML may be simply modified to yield a 2D-BDML estimator of the target bearing for cases in which the contribution to the beamspace outputs due to specular multipath is either nonexistent or negligible. This may be the case when either the target is at an elevation of a couple of beamwidths above broadside, corresponding to the initial stages of tracking in certain applications, or when the sea surface is very rough. Although the symmetric 3D-BDML estimator still performs properly under these conditions, as is shown in Section IV, higher quality estimates may be obtained by employing the 2D-BDML estimator. This is demonstrated and explained in Section VI. On the other hand, the 2D-BDML estimator performs rather poorly when a specular multipath component is present in the mainlobe of either of the two beams.

In heuristic terms, the 2D-BDML estimator is effectively derived from the nonsymmetric 3D-BDML estimator by shutting off the beam pointed to $u = u_c - 2/M$. u_c is then chosen to be an angle in the general vicinity of the pointing angle of the transmission beam. The transformation from element space to beamspace is accomplished by applying the $M \times 2$ matrix beamformer

$$\mathbf{S}_M^r = \left[\mathbf{a}_M(u_c) : \mathbf{a}_M\left(u_c + \frac{2}{M}\right)\right] \tag{33}$$

to each snapshot; the superscript r stands for reduced dimension. This produces the 2×1 beamspace snapshot vectors $\mathbf{x}_B^r(n) = \mathbf{S}_M^{rH}\mathbf{x}(n)$, $n = 1,\ldots,N$, from which the 2×2 beamspace correlation matrix is formed as $\hat{\mathbf{R}}_{bb}^r = (1/N)\sum_{n=1}^{N}\mathbf{x}_B^r(n)\mathbf{x}_B^{rH}(n)$. Again, we are primarily concerned with $N = 1$.

A development similar to that which lead to the nonsymmetric 3D-BDML bearing estimation scheme yields a similar two-step procedure. In the first step, $\mathbf{v}^r = [v_1^r, v_2^r]$ is computed as the eigenvector of $\mathrm{Re}\{\hat{\mathbf{R}}_{bb}^r\}$ associated with the smallest eigenvalue. In the second step, $\hat{u}_1$ is determined as that value of u, in the vicinity of the angular region encompassed by the mainlobes of the two beams, satisfying $\mathbf{v}^{rT}\mathbf{b}^r(u_1) = 0$, where $\mathbf{b}^r(u_1) = \mathbf{S}_M^{rH}\mathbf{a}_M(u_1)$. Similar to the case with nonsymmetric 3D-BDML, the second step may be formulated in terms of the root of a simple linear equation. This is accomplished by observing that the $(M-1)$th order polynomial formed using the first column of $\mathbf{S}_M^r$ as the coefficient vector has $M-2$ roots in common with that using the second column. In addition to the $M-3$ common roots $z_m = e^{j\pi(u_c+(2m/M))}$, $m = 2,\ldots,M-2$ cited previously, these two polynomials each have a root at $z = e^{j\pi(u_c-(2/M))}$ as well. Let $d(z) = d_0 + d_1 z$ be the linear polynomial for which $\hat{z}_1 = e^{j\pi\hat{u}_1}$ is the root. It is easy to verify that $d(z)$ may be obtained via the polynomial division

$$d(z) = d_0 + d_1 z = \frac{q_0 + q_1 z + q_0^* z^2}{z - e^{j\pi(u_c-(2/M))}} \tag{34}$$

where q_0 and q_1 are given by (24) with $v_1 = 0$, $v_1^r = v_2$, and $v_2^r = v_3$, i.e.,

$$\begin{aligned} q_0 &= e^{j\pi u_c}\left\{v_2^r - v_1^r e^{-j(\pi/M)}\right\}; \\ q_1 &= 2v_1^r\cos\left(\frac{\pi}{M}\right) - 2v_2^r\cos\left(\frac{2\pi}{M}\right). \end{aligned} \tag{35}$$

Cross-multiplying by $z - e^{j\pi(u_c-(2/M))}$ in (34) and equating the coefficients of z^0 and z^2 on both sides yields the relationships

$$-d_0 e^{j\pi(u_c-(2/M))} = q_0; \qquad d_1 = q_0^*. \tag{36}$$

Now, the root of $d_0 + d_1 z$ is simply $\hat{z}_1 = -d_0/d_1$. Invoking the relationships in (36), this root may be expressed as

$$\hat{z}_1 = -\frac{d_0}{d_1} = e^{j\pi(-u_c+(2/M))}\frac{q_0}{q_0^*}. \tag{37}$$

It is obvious from this equation that $\hat{z}_1$ lies on the unit circle. As the phase angle of $\hat{z}_1$ is $\pi\hat{u}_1$, (37) dictates

$$\hat{u}_1 = -u_c + \frac{2}{M} + \frac{1}{\pi}2\arg\{q_0\} \tag{38}$$

$\arg\{q_0\}$ is simply determined by manipulating the expression for q_0 in (35)

$$\begin{aligned} q_0 &= e^{j\pi u_c}e^{-j(\pi/2M)}\left\{-v_1^r e^{-j(\pi/2M)} + v_2^r e^{j(\pi/2M)}\right\} \\ &= e^{j\pi u_c}e^{-j(\pi/2M)}\left\{(v_1^r - v_2^r)\cos\left(\frac{\pi}{2M}\right)\right. \\ &\qquad \left. + j(v_2^r + v_1^r)\sin\left(\frac{\pi}{2M}\right)\right\} \end{aligned}$$

such that

$$\arg\{q_0\} = \pi u_c - \frac{\pi}{2M} + \tan^{-1}\left\{\left[\frac{v_1^r + v_2^r}{v_1^r - v_2^r}\right]\tan\left(\frac{\pi}{2M}\right)\right\}. \tag{39}$$

Substitution of (39) in (38) yields

$$\hat{u}_1 = u_c + \frac{1}{M} + \frac{2}{\pi}\tan^{-1}\left\{\left[\frac{v_1^r + v_2^r}{v_1^r - v_2^r}\right]\tan\left(\frac{\pi}{2M}\right)\right\} \tag{40}$$

where $\mathbf{v}^r = [v_1^r, v_2^r]$ is the eigenvector of $\mathrm{Re}\{\hat{\mathbf{R}}_{bb}^r\}$ associated with the smallest eigenvalue. Note that the angle $u = u_c + 1/M$ is the midpoint between the pointing angles of the two beams, u_c and $u_c + 2/M$.

IV. EFFECTS OF FORWARD-BACKWARD AVERAGING IN SYMMETRIC 3D-BDML

Recall that $\Delta\Psi$ denotes the phase difference between the direct and specular path signals at the center of the array. We here demonstrate analytically that nonsymmetric 3D-BDML breaks down when $\Delta\Psi$ is either 0° or 180° while symmetric 3D-BDML exhibits no such breakdown phenomenon. Let ρ denote the magnitude of the reflection coefficient; for a smooth surface of reflection $\rho \approx 0.9$ [19]. The expected value of the 3×3 sample beamspace correlation matrix, $\mathbf{R}_{bb}$, defined in (18) has the form

$$\mathbf{R}_{bb} = E\left\{\frac{1}{N}\sum_{n=1}^{N}\mathbf{x}_B(n)\mathbf{x}_B^H(n)\right\} = \mathbf{B}\mathbf{R}_{ss}\mathbf{B}^T + \sigma_{bn}^2\mathbf{I}_3 \tag{41}$$

where σ_{bn}^2 is the mean square value of the noise present at each of the three beamspace ports and

$$\begin{aligned} \mathbf{R}_{ss} &= \frac{1}{N}\sum_{n=1}^{N}\mathbf{c}(n)\mathbf{c}^H(n) = \begin{bmatrix} \overline{\sigma}_1^2 & \rho e^{-j\Delta\Psi}\overline{\sigma}_1^2 \\ \rho e^{j\Delta\Psi}\overline{\sigma}_1^2 & \rho^2\overline{\sigma}_1^2 \end{bmatrix} \\ &= \overline{\sigma}_1^2\begin{bmatrix} 1 \\ \rho e^{j\Delta\Psi} \end{bmatrix}\left[1, \rho e^{-j\Delta\Psi}\right] \end{aligned} \tag{42}$$

$\mathbf{c}(n) = [c_1(n), c_2(n)]^T$ as prescribed previously in (6) and $\overline{\sigma}_1^2 = (1/N)\sum_{n=1}^{N}|c_1(n)|^2$. Recall that $c_1(n)$ and

$c_2(n)$ are here viewed as deterministic but unknown sequences. Also, the form of $\mathbf{R}_{ss}$ in (42) assumes that ρ and $\Delta\Psi$ are constant over the interval in which the N snapshots are collected; the basic assumption is that N is small, typically one as implied by the term "monopulse".

In nonsymmetric 3D-BDML, $\mathbf{v}$ is computed as the eigenvector of $\mathrm{Re}\{\hat{\mathbf{R}}_{bb}\}$ associated with the smallest eigenvalue. Recall that $\mathbf{B}$ is real such that

$$\mathrm{Re}\{\mathbf{R}_{bb}\} = \mathbf{B}\,\mathrm{Re}\{\mathbf{R}_{ss}\}\mathbf{B}^T + \sigma_{bn}^2\mathbf{I}_3 \tag{43}$$

where

$$\mathrm{Re}\{\mathbf{R}_{ss}\} = \overline{\sigma}_1^2\begin{bmatrix} 1 & \rho\cos(\Delta\Psi) \\ \rho\cos(\Delta\Psi) & \rho^2 \end{bmatrix}. \tag{44}$$

We state without proof some important properties with regard to the eigenstructure of $\mathrm{Re}\{\mathbf{R}_{bb}\}$. The proof of each of these properties is straightforward and may be found in [22]. First, the smallest eigenvalue of $\mathrm{Re}\{\mathbf{R}_{bb}\}$, denoted $\lambda_{\min}^{rb}$, is equal to σ_{nb}^2. Second, if $\mathrm{Re}\{\mathbf{R}_{ss}\}$ is of rank two, the eigenvector of $\mathrm{Re}\{\mathbf{R}_{bb}\}$ associated with $\lambda_{\min}^{rb} = \sigma_{nb}^2$ is orthogonal to both $\mathbf{b}(u_1)$ and $\mathbf{b}(u_2)$. Thus, if $\mathrm{Re}\{\mathbf{R}_{ss}\}$ is of rank two, execution of nonsymmetric 3D-BDML with either the expected value or the noiseless version of $\hat{\mathbf{R}}_{bb}$ provides the true values of u_1 and u_2. Observing (44), $\mathrm{Re}\{\mathbf{R}_{ss}\}$ is of full rank equal to 2 so long as $\Delta\Psi$ does not equal to either $0°$ or $180°$. In these two cases, $\mathrm{Re}\{\mathbf{R}_{ss}\}$ is of rank 1 such that the smallest eigenvalue $\lambda_{\min}^{rb} = \sigma_{nb}^2$ is of multiplicity 2 and the corresponding 2-D eigenspace is orthogonal to the 1-D space spanned by $\mathbf{b}(u_1) \pm \rho\mathbf{b}(u_2)$, where "+" is for the case $\Delta\Psi = 0°$ and "−" is for the case $\Delta\Psi = 180°$. Under either of these two conditions, neither of the two vectors chosen to span the 2-D eigenspace associated with $\lambda_{\min}^{rb} = \sigma_{nb}^2$ is orthogonal to $\mathbf{b}(u_1)$ and $\mathbf{b}(u_2)$ individually. Thus, the method breaks down when either $\Delta\Psi = 0°$ or $\Delta\Psi = 180°$. This phenomenon is demonstrated in the simulations presented in Section VI.

We next consider the execution of symmetric 3D-BDML when supplied with either the expected value or the noiseless version of $\hat{\mathbf{R}}_{bb}$. In the first analysis, we consider u_c to be exactly equal to the bisector angle u_B. Symmetric 3D-BDML dictates that $\mathbf{v}$ be computed as that centro-symmetric eigenvector of $\mathrm{Re}\{\hat{\mathbf{R}}_{bb}^{fb}\}$ associated with the smaller eigenvalue, where $\hat{\mathbf{R}}_{bb}^{fb}$ is defined in (29). Recall that with $u_c = u_B$, the two columns of $\mathbf{B}$ are related according to $\mathbf{b}(u_2) = \tilde{\mathbf{I}}_3\mathbf{b}(u_1)$ such that $\tilde{\mathbf{I}}_3\mathbf{B}\tilde{\mathbf{I}}_2 = \mathbf{B}$. Exploitation of this property yields

$$\begin{aligned}\mathrm{Re}\{\mathbf{R}_{bb}^{fb}\} &= \tfrac{1}{2}\mathrm{Re}\left\{\mathbf{R}_{bb} + \tilde{\mathbf{I}}_3\mathbf{R}_{bb}\tilde{\mathbf{I}}_3\right\} \\ &= \tfrac{1}{2}\left\{\mathbf{B}\,\mathrm{Re}\{\mathbf{R}_{ss}\}\mathbf{B}^T + \tilde{\mathbf{I}}_3\mathbf{B}\tilde{\mathbf{I}}_2\tilde{\mathbf{I}}_2\,\mathrm{Re}\{\mathbf{R}_{ss}\}\tilde{\mathbf{I}}_2\tilde{\mathbf{I}}_2\mathbf{B}^T\tilde{\mathbf{I}}_3\right\} \\ &\quad + \sigma_{bn}^2\mathbf{I}_3 = \mathbf{B}\tfrac{1}{2}\mathrm{Re}\left\{\mathbf{R}_{ss} + \tilde{\mathbf{I}}_2\mathbf{R}_{ss}\tilde{\mathbf{I}}_2\right\}\mathbf{B}^T + \sigma_{bn}^2\mathbf{I}_3\end{aligned} \tag{45}$$

where we have invoked the property $\tilde{\mathbf{I}}_2\tilde{\mathbf{I}}_2 = \mathbf{I}_2$. Thus, $\mathrm{Re}\{\mathbf{R}_{bb}^{fb}\}$ can be expressed in the form $\mathbf{B}\,\mathrm{Re}\{\mathbf{R}_{ss}^{fb}\}\mathbf{B}^T + \sigma_{bn}^2\mathbf{I}_3$, where

$$\begin{aligned}\mathbf{R}_{ss}^{fb} &= \frac{1}{2}\left\{\mathbf{R}_{ss} + \tilde{\mathbf{I}}_2\mathbf{R}_{ss}\tilde{\mathbf{I}}_2\right\} \\ &= \overline{\sigma}_1^2\begin{bmatrix} \dfrac{1+\rho^2}{2} & \rho\cos\Delta\Psi \\ \rho\cos\Delta\Psi & \dfrac{1+\rho^2}{2} \end{bmatrix}\end{aligned} \tag{46}$$

where we have substituted (42) for $\mathbf{R}_{ss}$. In contrast to the situation with $\mathrm{Re}\{\mathbf{R}_{ss}\}$ in (44), which is of rank one for all values of ρ when $\Delta\Psi$ is either $0°$ or $180°$, $\mathbf{R}_{ss}^{fb}$ is of rank two except when either $\Delta\Psi = 0°$ and, at the same time, $\rho = 1$, or when $\Delta\Psi = 180°$ and, at the same time, $\rho = 1$. That is, denoting $\rho_c = \rho e^{j\Delta\Psi}$, the only values of ρ_c for which $\mathbf{R}_{ss}^{fb}$ in (46) is of rank one are $\rho_c = 1$ or $\rho_c = -1$. Thus, as long as ρ_c is neither 1 or -1, execution of symmetric 3D-BDML in the asymptotic or noiseless cases provides the true value of u_1.

As a practical matter, the magnitude of ρ_c, ρ, is always less than one due to losses incurred at the surface of reflection [19]. Notwithstanding, symmetric 3D-BDML does not break down when $\Delta\Psi = 0°$ and $\rho = 1$, i.e., when $\rho_c = 1$, despite the rank deficiency problem. In this case, $\mathbf{B}\,\mathrm{Re}\{\mathbf{R}_{ss}^{fb}\}\mathbf{B}^T$ is of rank one such that the smallest eigenvalue of $\mathrm{Re}\{\mathbf{R}_{bb}^{fb}\}$, $\lambda_{\min}^{rb} = \sigma_{nb}^2$, is of multiplicity 2 and the corresponding 2-D eigenspace is orthogonal to the 1-D space spanned by $\mathbf{b}(u_1) + \mathbf{b}(u_2) = \mathbf{b}(u_1) + \tilde{\mathbf{I}}_3\mathbf{b}(u_1)$. Since $\mathbf{b}(u_1) + \tilde{\mathbf{I}}_3\mathbf{b}(u_1)$ is centro-symmetric, one of the eigenvectors associated with $\lambda_{\min}^{rb} = \sigma_{nb}^2$ is centro-symmetric while the other is centro-antisymmetric. In accordance with symmetric 3D-BDML, $\mathbf{v}$ is chosen as the centro-symmetric eigenvector associated with $\lambda_{\min}^{rb} = \sigma_{nb}^2$. Invoking the centro-symmetry of $\mathbf{v}$ yields

$$\begin{aligned}\mathbf{v}^T\{\mathbf{b}(u_1) + \mathbf{b}(u_2)\} &= \mathbf{v}^T\{\mathbf{b}(u_1) + \tilde{\mathbf{I}}_3\mathbf{b}(u_1)\} \\ &= 2\mathbf{v}^T\mathbf{b}(u_1) = 0\end{aligned} \tag{47}$$

which indicates that $\mathbf{v}$ is orthogonal to $\mathbf{b}(u_1)$. This implies that in the asymptotic or no noise cases, symmetric 3D-BDML provides the true value of u_1 even in the extreme case of $\Delta\Psi = 0°$ and $\rho = 1$.

Note that the argument above signified by (47) does not work for the case of $\Delta\Psi = 180°$ and $\rho = 1$, i.e., $\rho_c = -1$. Symmetric 3D-BDML breaks down under these extreme conditions. In general, poor performance is obtained in the case of $\Delta\Psi = 180°$ when $\rho \approx 1$. The use of frequency diversity to overcome this problem is explored in the next section.

A. Operation With No Specular Multipath

The previous analysis provides a simple means for examining how symmetric 3D-BDML performs

when no specular multipath component is present. The absence of a specular multipath component is signified by setting ρ equal to zero. With $\rho = 0$ in (45) and (46), $\mathrm{Re}\{\mathbf{R}_{bb}^{fb}\}$ may be expressed as $\mathbf{B}\mathrm{Re}\{\mathbf{R}_{ss}^{fb}\}\mathbf{B}^T + \sigma_{bn}^2\mathbf{I}_3$, where $\mathbf{R}_{ss}^{fb} = \frac{1}{2}\bar{\sigma}_1^2\mathbf{I}_2$ and

$$\mathbf{B} = \left[\mathbf{b}(u_1)\vdots\tilde{\mathbf{I}}_3\mathbf{b}(u_1)\right] = \left[\mathbf{b}(u_1)\vdots\tilde{\mathbf{I}}_3\mathbf{b}(2u_c - u_1)\right] \quad (48)$$

where we have invoked the property of $\mathbf{b}(u)$ described by (12). It is deduced that despite the absence of specular multipath, the process of forward-backward averaging according to (29) effectively creates an artificial source at $u = 2u_c - u_1$ of equal power. Thus, even without a specular multipath component present, symmetric 3D-BDML must nevertheless resolve two sources angularly separated by $|u_1 - (2u_c - u_1)| = 2|u_c - u_1|$. Hence, the closer u_c is to u_1, the "harder" symmetric 3D-BDML must work to resolve the actual source and the artificial source. This phenomenon is illustrated in simulations presented in Section VI. Nevertheless, since $\mathbf{R}_{ss}^{fb} = \frac{1}{2}\bar{\sigma}_1^2\mathbf{I}_2$ is of rank 2, it follows that in the asymptotic or no noise cases symmetric 3D-BDML provides the true value of u_1.

B. Effect of Error in Bisector Angle Estimate

The formula for the bisector angle given by (4) was based on a flat-Earth model and the approximation that $\cos(\alpha) = \cos(\theta_2) \approx 1$. In the case of a spherical Earth model, the bisector angle is approximated as the angle from the array center to a point directly under the target on the plane tangent to the surface of the Earth at the point of reflection, computed for a target height equal to the radar height. Although the bisector angle estimates provided by these procedures are quite accurate, an assessment of the sensitivity of symmetric 3D-BDML to an error in the bisector angle estimate is in order. Although symmetric 3D-BDML is a nonlinear estimator, a simple analysis leads to the intuitively satisfying conjecture that an error in the bisector angle estimate translates into a bias in the symmetric 3D-BDML estimator of the same magnitude. The argument is as follows.

Consider $u_c \neq u_B$ such that $u_c = u_B + \delta$. It is assumed that the deviation δ is a very small fraction of a beamwidth, i.e, $\delta \ll 2/M$. Now, since u_B is the true bisector angle, $u_1 = u_B + \Delta$ and $u_2 = u_B - \Delta$. Invoking the property of $\mathbf{b}(u)$ in (12) yields

$$\begin{aligned}\tilde{\mathbf{I}}_3\mathbf{b}(u_1) &= \mathbf{b}(2u_c - u_1) = \mathbf{b}(2u_B + 2\delta - u_B - \Delta)\\ &= \mathbf{b}(u_B - \Delta + 2\delta) = \mathbf{b}(u_2 + 2\delta). \quad (49)\end{aligned}$$

Similarly, $\tilde{\mathbf{I}}_3\mathbf{b}(u_2) = \mathbf{b}(u_1 + 2\delta)$. Hence, in the case of $u_c \neq u_B$, the expected value of $\mathrm{Re}\{\mathbf{R}_{bb}^{fb}\}$ may be expressed as

$$\begin{aligned}\mathrm{Re}\{\mathbf{R}_{bb}^{fb}\} &= \tfrac{1}{2}\left[\mathbf{b}(u_1)\vdots\mathbf{b}(u_2)\right]\mathrm{Re}\{\mathbf{R}_{ss}\}\left[\mathbf{b}(u_1)\vdots\mathbf{b}(u_2)\right]^T\\ &\quad + \tfrac{1}{2}\left[\mathbf{b}(u_2 + 2\delta)\vdots\mathbf{b}(u_1 + 2\delta)\right]\mathrm{Re}\{\mathbf{R}_{ss}\}\\ &\quad \times \left[\mathbf{b}(u_2 + 2\delta)\vdots\mathbf{b}(u_1 + 2\delta)\right]^T + \sigma_{bn}^2\mathbf{I}_3. \quad (50)\end{aligned}$$

The forward-backward averaging process has effectively created two artificial sources, one at $u = u_1 + 2\delta$ and another at $u = u_2 + 2\delta$. As $\rho \approx 1$, the four sources, the two actual sources and the two artificial ones, are of nearly equal strength. In the practical case where δ is a very small fraction of a beamwidth, it is conjectured that symmetric 3D-BDML cannot resolve the actual source at $u = u_1$ and the artificial source at $u = u_1 + 2\delta$ and, in light of their equal power, yields (on average) an estimate equal to the center value of $u = u_1 + \delta$. This, in turn, leads to the conjecture that an error in the bisector angle estimate translates into a bias in the symmetric 3D-BDML estimator of the same magnitude. This conjecture is validated by simulations presented in Section VI.

V. FREQUENCY DIVERSITY

Advances in radar technology have progressed to the point where the use of frequency diversity in tracking systems has become increasingly more commonplace. Depending on the system hardware, the pulses at the various frequencies may be transmitted simultaneously and/or in rapid succession corresponding to frequency hopping. An example of a real radar system where frequency diversity is employed is the multiparameter adaptive radar system (MARS) described by V. Kezys and S. Haykin [18]. This experimental bistatic radar array consists of a 32-element, horizontally polarized linear array operating coherently over the band 8.05 to 12.36 GHz. Each antenna element is followed by two receiver channels allowing for simultaneous reception on two separate frequencies: one fixed at 10.2 GHz and the other agile over the band 8.05 to 12.36 GHz in 30 MHz steps. We cite the MARS radar system as an example of what is feasible in the way of multifrequency transmission with current technology.

There are a number of advantages to employing frequency diversity for tracking purposes. For our purposes here, frequency diversity translates into phase diversity, i.e., diversity in the phase difference occurring at the center of the array. Accordingly, multifrequency operation diminishes the pejorative effect of a 180° phase difference at any one transmission frequency. With judicious processing, the use of multiple frequencies also allows us to achieve a large effective signal-to-noise ratio (SNR). This is accomplished by coherently combining the

additive component of the 3×3 beamspace correlation matrix at each frequency due solely to the direct and specular path signals; the additive components of the beamspace correlation matrix at each frequency due to receiver noise and cross-products between signal and noise are incoherently combined. The coherent combination of the signal-only (no noise) component of the beamspace correlation matrix at each frequency is accomplished through the use of focusing transformations in accordance with the coherent signal subspace (CSS) processing method of Wang and Kaveh [20–21]. A multifrequency version of 3D-BDML incorporating CSS is developed below.

A discussion of multifrequency operation requires the introduction of some notation. The transmission frequencies are denoted f_j, $j = 1,\ldots,J$, where J is the total number of such frequencies. f_0 denotes the frequency for which the M elements of the array are spaced by a half-wavelength; f_0 may or may not be one of the transmission frequencies. At frequency f_j, we allow the option of operating with an array of M_j contiguous elements extracted from the overall array of M elements. The formulation is general; M_j may be equal to M or it may be less than M. There are two advantages to operating with an effective subaperture equal to that associated with a subarray of M_j elements at frequency f_j. First, it leads to a criterion for the selection of transmission frequencies which makes the job of coherently combining the signal-only component of $\mathbf{R}_{bb}(f_j)$, the 3×3 beamspace correlation matrix formed at f_j, a very simple procedure. This criterion is discussed shortly. Second, with $M_j < M$, there are $M - M_j + 1$ identical subarrays of $M_j < M$ contiguous elements allowing for spatial smoothing [15] at frequency f_j. The process of spatial smoothing in addition to CSS processing further diminishes the sensitivity of 3D-BDML to the phase difference at any one frequency.

The element space manifold vector/classical beamforming vector associated with frequency f_j and a subarray of M_j contiguous elements is denoted $\mathbf{a}_{M_j}(u;f_j)$. $\mathbf{a}_M(u)$ in (2), now denoted $\mathbf{a}_M(u;f_0)$, is easily generalized for arbitrary frequencies of operation and subarrays of length M_j:

$$\mathbf{a}_{M_j}(u;f_j) = \left[e^{-j\pi(M_j-1)/2(f_j/f_0)u}, e^{-j\pi(M_j-3)/2(f_j/f_0)u}, \ldots, 1, \ldots, e^{j\pi(M_j-3)/2(f_j/f_0)u}, e^{j\pi(M_j-1)/2(f_j/f_0)u}\right]^T \quad \text{if } M_j \text{ is odd}$$

$$\mathbf{a}_{M_j}(u;f_j) = \left[e^{-j\pi(M_j-1)/2(f_j/f_0)u}, \ldots, e^{-j\pi(f_j/2f_0)u}, e^{j\pi(f_j/2f_0)u}, \ldots, e^{j\pi(M_j-1)/2(f_j/f_0)u}\right]^T \quad \text{if } M_j \text{ is even.} \tag{51}$$

Let $\mathbf{S}_{M_j}(f_j)$ denote the $M_j \times 3$ beamformer to be applied to each of $M - M_j + 1$ identical subarrays of $M_j < M$ contiguous elements at frequency f_j.

$$\mathbf{S}_{M_j}(f_j) = \frac{1}{\sqrt{M_j}}\left[\mathbf{a}_{M_j}\left(u_c - \frac{f_0}{f_j}\frac{2}{M_j}; f_j\right) \vdots \mathbf{a}_{M_j}(u_c; f_j) \vdots \mathbf{a}_{M_j}\left(u_c + \frac{f_0}{f_j}\frac{2}{M_j}; f_j\right)\right] \quad j = 1,\ldots,J. \tag{52}$$

Given the definition of $\mathbf{a}_{M_j}(u;f_j)$ in (51), it is easily verified that the columns of $\mathbf{S}_{M_j}(f_j)$ are mutually orthonormal. It is also easily verified that each of the three polynomials formed with a particular column of $\mathbf{S}_{M_j}(f_j)$ as the corresponding coefficients has $M_j - 3$ roots in common with the other two polynomials.

The first step in multifrequency 3D-BDML incorporating CSS is to form a spatially smoothed [15], beamspace correlation matrix, denoted $\tilde{\mathbf{R}}_{bb}(f_j)$, at each frequency in the following manner. The overall array is decomposed into $M - M_j + 1$ overlapping subarrays of $M_j < M$ contiguous elements. $\mathbf{S}_{M_j}(f_j)$ is applied to each subarray, and $\tilde{\mathbf{R}}_{bb}(f_j)$ is formed as the arithmetic mean of the outer products of the $M - M_j + 1$ 3×1 beamspace snapshot vectors thus created. The second step is to apply a focusing transformation on both the left and right of each $\tilde{\mathbf{R}}_{bb}(f_j)$, $j = 1,\ldots,J$, so that the signal-only component of each may be coherently combined at some common frequency. Let the common frequency be f_k, where $f_k \in \{f_1, f_2, \ldots, f_J\}$. The focusing transformation to be applied to $\tilde{\mathbf{R}}_{bb}(f_j)$ is denoted $\mathbf{T}_j^k$, $j = 1,\ldots,J$. As $f_k \in \{f_1, f_2, \ldots, f_J\}$, the notation implies $\mathbf{T}_k^k = \mathbf{I}_3$. We quantify the role of the focusing transformations more precisely as well as discuss methods for constructing such shortly. Given the appropriate set of focusing transformations, the CSS averaged correlation matrix, denoted $\{\overline{\mathbf{R}}_{bb}\}$, is computed via the simple sum

$$\overline{\mathbf{R}}_{bb} = \frac{1}{J}\sum_{j=1}^{J} \mathbf{T}_j^k \tilde{\mathbf{R}}_{bb}(f_j)\mathbf{T}_j^{kT}. \tag{53}$$

A summary of the multifrequency version of nonsymmetric 3D-BDML is then as follows. Compute $\mathbf{v} = [v_1, v_2, v_3]^T$ as that eigenvector of $\mathrm{Re}\{\overline{\mathbf{R}}_{bb}\}$, computed in the metric $\overline{\mathbf{T}} = 1/J\sum_{j=1}^{J}\mathbf{T}_i^k\mathbf{T}_i^{kT}$, associated with the smallest eigenvalue. Form the coefficients of the quadratic equation $q(z)$ according to

$$q_0 = e^{j\pi u_c}\left\{-v_1 e^{-j(f_0/f_k)(\pi/M_k)} + v_2 - v_3 e^{j(f_0/f_k)(\pi/M_k)}\right\} = q_2^* \tag{54a}$$

$$q_1 = 2(v_1 + v_3)\cos\left(\frac{f_0}{f_k}\frac{\pi}{M_k}\right) - 2v_2\cos\left(\frac{f_0}{f_k}\frac{2\pi}{M_k}\right) \tag{54b}$$

where the scaling factor f_0/f_k accounts for operation at a frequency other than that for which the elements

are spaced by a half-wavelength. Next, compute z_1 and z_2 as the two roots of $q(z)$. The estimates of u_1 and u_2 are then $\hat{u}_1 = (f_0/f_k)(1/j\pi)\ln\{z_1\}$ and $\hat{u}_2 = (f_0/f_k)(1/j\pi)\ln\{z_2\}$.

The multifrequency version of symmetric 3D-BDML is similar except that $\overline{\mathbf{R}}_{bb}$ is replaced by $\overline{\mathbf{R}}_{bb}^{fb} = \frac{1}{2}\{\overline{\mathbf{R}}_{bb} + \tilde{\mathbf{I}}_3\overline{\mathbf{R}}_{bb}\tilde{\mathbf{I}}_3\}$. $\mathbf{v} = [v_1, v_2, v_1]^T$ is computed as that centro-symmetric eigenvector of $\mathrm{Re}\{\overline{\mathbf{R}}_{bb}^{fb}\}$, in the metric $\overline{\mathbf{T}} = 1/J\sum_{j=1}^{J}\mathbf{T}_j^k\mathbf{T}_j^{kT}$, associated with the smaller eigenvalue. With $v_3 = v_1$ in (54), the remaining steps are the same. Of course, use of symmetric 3D-BDML implies that u_c in (52) is equal to an estimate of bisector angle.

With the phase diversity achieved with frequency diversity, one might question the need for symmetric 3D-BDML in the case of multifrequency operation. Of course, the differential in performance between the symmetric and nonsymmetric cases will depend on the specific values and total number of frequencies employed. For most practical applications in which the number of transmission frequencies is rather small (2, 3, or 4) and the inter-frequency spacings not so great, symmetric 3D-BDML can be expected to significantly outperform nonsymmetric 3D-BDML. Simulations are presented in the next Section backing this claim.

To quantify the role of $\mathbf{T}_j^k$ more precisely, let $\mathbf{b}(u;f_j)$ denote the 3×1 beamspace manifold vector associated with frequency f_j, i.e., $\mathbf{b}(u;f_j) = \mathbf{S}_{M_j}^H(f_j)\mathbf{a}_{M_j}(u;f_j)$, $j = 1,\ldots,J$. Given the definitions of $\mathbf{a}_{M_j}(u;f_j)$ and $\mathbf{S}_{M_j}(f_j)$ in (51) and (52), respectively, it is easy to verify the following component-wise expression for $\mathbf{b}(u;f_j)$

$$\begin{aligned}\mathbf{b}(u;f_j) &= \mathbf{S}_{M_j}^H(f_j)\mathbf{a}_{M_j}(u;f_j)\\ &= \frac{1}{M_j}\left[\frac{\sin\left(M_j\frac{\pi}{2}\frac{f_j}{f_0}\left(u-u_c+\frac{f_0}{f_j}\frac{2}{M_j}\right)\right)}{\sin\left(\frac{\pi}{2}\frac{f_j}{f_0}\left(u-u_c+\frac{f_0}{f_j}\frac{2}{M_j}\right)\right)},\right.\\ &\qquad \frac{\sin\left(M_j\frac{\pi}{2}\frac{f_j}{f_0}(u-u_c)\right)}{\sin\left(\frac{\pi}{2}\frac{f_j}{f_0}(u-u_c)\right)},\\ &\qquad \left.\frac{\sin\left(M_j\frac{\pi}{2}\frac{f_j}{f_0}\left(u-u_c-\frac{f_0}{f_j}\frac{2}{M_j}\right)\right)}{\sin\left(\frac{\pi}{2}\frac{f_j}{f_0}\left(u-u_c-\frac{f_0}{f_j}\frac{2}{M_j}\right)\right)}\right]^T.\end{aligned} \tag{55}$$

Further, define $\mathbf{B}(f_j) = [\mathbf{b}(u_1;f_j)\vdots\mathbf{b}(u_2;f_j)]$, $j = 1,\ldots,J$. In accordance with the CSS methodology of Wang and Kaveh, the focusing matrices must satisfy

$$\mathbf{B}(f_k) = \mathbf{T}_j^k\mathbf{B}(f_j), \qquad j = 1,\ldots,J. \tag{56}$$

Again, $\mathbf{T}_k^k = \mathbf{I}_3$. In general, construction of the appropriate set of focusing matrices satisfying (56) requires knowledge of u_1 and u_2, i.e., the angles we are trying to estimate. Accordingly, Wang and Kaveh [20–21] propose an iterative procedure which commences with an initial set of focusing matrices based on some coarse estimates of the angles. One possibility for initialization is to take the pointing angle of the center beam u_c as an estimate of both angles. In a tracking situation, it makes sense to use the most recent bearing estimates as the initial estimates. Proceeding with the initial set of focusing matrices yields updated estimates of the angles corresponding to the first iteration. The new pair of angles are used to construct an updated set of focusing matrices which, in turn, yield the estimates of the angles at the second iteration. This procedure is iterated until the absolute value of the difference between respective angle estimates obtained at the $(k+1)$th and kth iterations is less than some threshold. A number of methods for constructing the focusing matrices have been proposed [20–21].

The need for focusing matrices in multifrequency 3D-BDML may be eliminated if the transmission frequencies, f_j, $j = 1,\ldots,J$, and corresponding subarray lengths, M_j, $j = 1,\ldots,J$, are selected such that the product f_jM_j is the same for each frequency, i.e., f_jM_j = constant, $j = 1,\ldots,J$. This assertion is justified by approximating each of the array patterns comprising the components of $\mathbf{b}(u;f_j)$ in (55) as a sinc function in the vicinity of the respective mainlobe and first few sidelobes:

$$\begin{aligned}\mathbf{b}(u;f_j) &= \mathbf{S}_{M_j}^H(f_j)\mathbf{a}_{M_j}(u;f_j)\\ &\approx \frac{f_0}{M_jf_j}\left[\frac{\sin\left(\frac{\pi}{2}\frac{M_jf_j}{f_0}\left(u-u_c+\frac{f_0}{f_j}\frac{2}{M_j}\right)\right)}{\left(\frac{\pi}{2}\left(u-u_c+\frac{f_0}{f_j}\frac{2}{M_j}\right)\right)},\right.\\ &\qquad \frac{\sin\left(\frac{\pi}{2}\frac{M_jf_j}{f_0}(u-u_c)\right)}{\left(\frac{\pi}{2}(u-u_c)\right)},\\ &\qquad \left.\frac{\sin\left(\frac{\pi}{2}\frac{M_jf_j}{f_0}\left(u-u_c+\frac{f_0}{f_j}\frac{2}{M_j}\right)\right)}{\left(\frac{\pi}{2}\left(u-u_c-\frac{f_0}{f_j}\frac{2}{M_j}\right)\right)}\right]^T.\end{aligned} \tag{57}$$

It is thus apparent that if $f_jM_j = \alpha$, $j = 1,\ldots,J$, the beamspace manifold vector $\mathbf{b}(u;f_j)$ is approximately identical, to a high degree of precision, for each transmission frequency!! With regard to (56), under these conditions $\mathbf{B}(f_k) \approx \mathbf{B}(f_j)$, $j = 1,\ldots,J$, eliminating the need for focusing matrices. In effect, with frequencies satisfying this criterion, the appropriate focusing matrices are identity matrices, i.e., $\mathbf{T}_j^k = \mathbf{I}_3$,

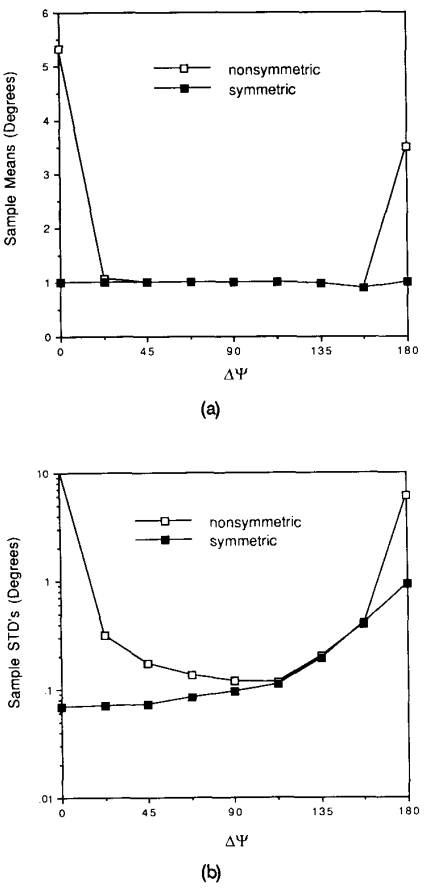

Fig. 3. Performance comparison: Nonsymmetric 3D-BDML versus symmetric 3D-BDML using true bisector angle. $M = 21$ elements and $N = 1$ snapshot. Direct path: $\theta_1 = 1°$ and SNR = 20 dB. Specular path: $\theta_2 = -1.5°$ and $\rho = 0.9$. Single frequency operation. SMEANs/SSTDs computed from 150 independent trials. (a) Direct path sample means. (b) Direct path sample STDs.

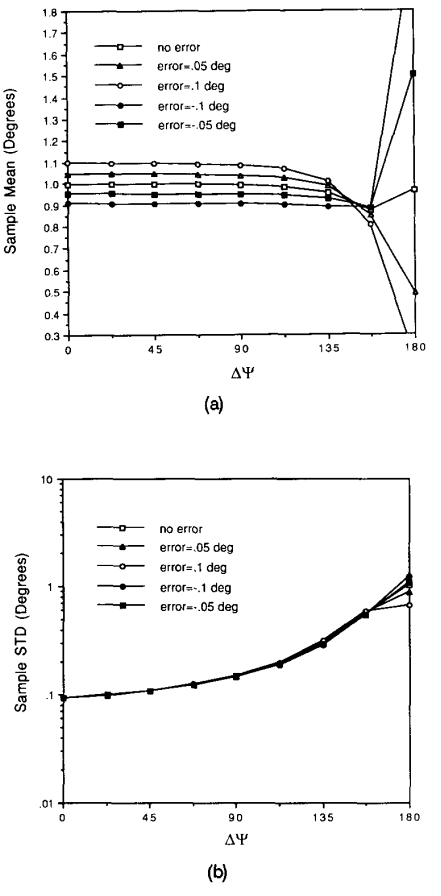

Fig. 4. Sensitivity of symmetric 3D-BDML to errors in the bisector angle estimate. Simulation parameters are same as those described in caption to Fig. 3. (a) Direct path sample means. (b) Direct path sample STDs.

$j = 1,\ldots,J$. Also, observing (54), it is apparent that with $f_j M_j = \alpha$, $j = 1,\ldots,J$, any of the transmission frequencies may serve as the reference frequency f_k. Hence, CSS averaging is simply accomplished by summing the spatially smoothed beamspace correlation matrices formed at each frequency. This represents a dramatic simplification.

Some practical issues with regard to the selection of transmission frequencies are discussed in Section VI. The sensitivity of this multifrequency method to deviations in the product $f_j M_j$ from frequency to frequency is examined as well.

VI. COMPUTER SIMULATIONS

Computer simulations were conducted to assess the performance of the various BDML bearing estimation schemes developed within in a simulated low-angle radar tracking environment. The following parameters were common to all test cases. First, the array employed was linear consisting of $M = 21$ elements uniformly-spaced by a half-wavelength at f_0. The nominal 3 dB beamwidth for this array is $\frac{2}{21}$ rads = 5.46°. The direct and specular path signals were angularly located at $\theta_1 = 1°$ and $\theta_2 = -1.5°$, respectively, corresponding to an angular separation of 0.46 beamwidths and a bisector angle of $\theta_B = -0.25°$. In the $u = \sin(\theta)$ domain, the relevant bisector quantity is $u_B = \frac{1}{2}\{\sin\theta_1 + \sin\theta_2\} = -0.00436$. The noise was additive, spatially white, and uncorrelated with the direct and specular path signals. The SNR of the direct path signal was 20 dB (per element). The ratio of the amplitude of the specular path signal to that of the direct path signal, ρ, was 0.9. In the case of single frequency operation at f_0, corresponding to the simulations presented in Figs. 3 through 5, each independent trial involved a single snapshot of data, $N = 1$. For each simulation example, the respective performance of the particular 3D-BDML algorithm employed was examined at nine equi-spaced values of $\Delta\Psi$, the phase difference between the direct and

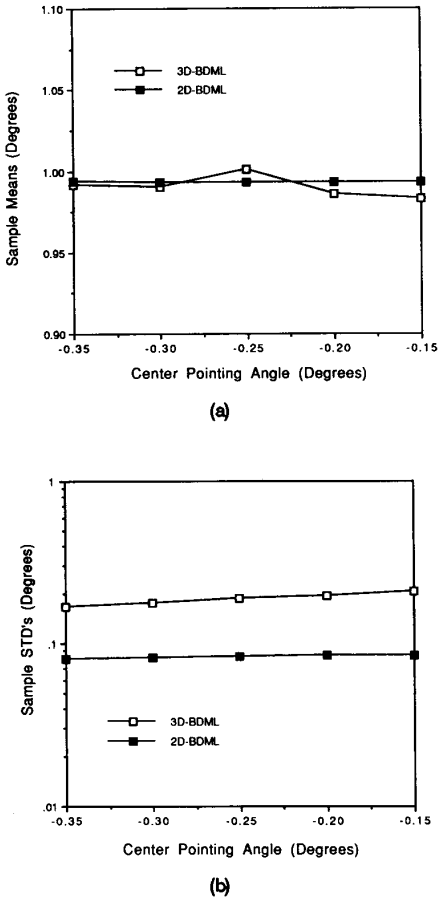

Fig. 5. Performance comparison: Symmetric 3D-BDML versus 2D-BDML as function of pointing angle of center beam in case of no specular multipath. Simulation parameters are same as those described in caption to Fig. 3 except $\rho = 0$. (a) Direct path sample means. (b) Direct path sample STDs.

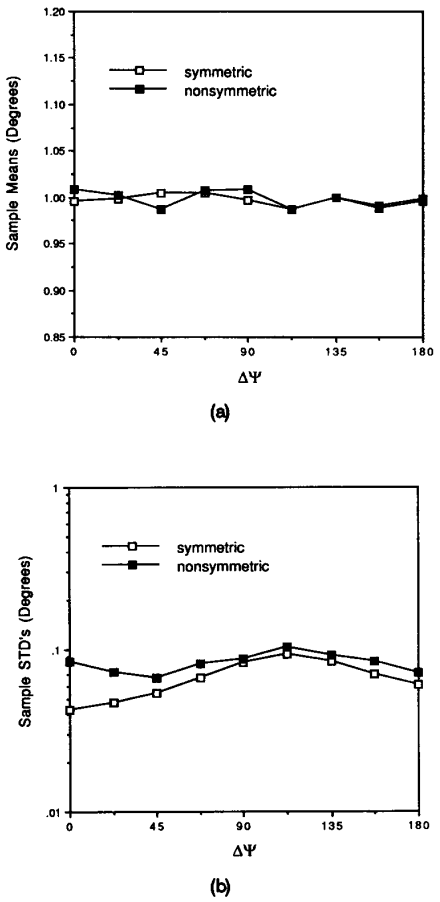

Fig. 6. Performance comparison: Nonsymmetric 3D-BDML versus symmetric 3D-BDML using the true bisector angle in the case of multifrequency operation. Simulation parameters are same as those described in caption to Fig. 3. Transmission frequencies: $f_1 = f_0$, $f_2 = \frac{21}{19} f_0$, and $f_3 = \frac{21}{17} f_0$, where f_0 denotes frequency for which elements are spaced by $\lambda/2$. $\Delta\Psi$ denotes phase difference at aperture center at f_0. (a) Direct path sample means. (b) Direct path sample STDs.

specular path signals at the center element at f_0, over the interval from 0° to 180°. Multifrequency operation with three frequencies satisfying $f_j M_j =$ constant, $j = 1,2,3$, is examined in Figs. 6 and 7. In this case, each independent trial involved the execution of the simplified multifrequency version of either symmetric 3D-BDML or nonsymmetric 3D-BDML given a single snapshot of data, $N = 1$, at each of the three frequencies. Finally, in all cases, sample means (SMEANs) and sample standard deviations (SSTDs) were computed from the results of 150 independent trials.

The first simulation results presented in Fig. 3 compare the performance of nonsymmetric 3D-BDML with that of symmetric 3D-BDML employing the actual bisector angle. The breakdown of nonsymmetric 3D-BDML in the respective cases of $\Delta\Psi = 0°$ and $\Delta\Psi = 180°$ is apparent. Interestingly enough, the performance achieved with $\Delta\Psi = 0°$ is worse than that achieved with $\Delta\Psi = 180°$. No such breakdown phenomenon is observed with the symmetric 3D-BDML estimator. However, the sample STD of the symmetric 3D-BDML estimator steadily increases from a value of 0.07° at $\Delta\Psi = 0°$ to a value of 0.94° at $\Delta\Psi = 180°$. The sample STD obtained with symmetric 3D-BDML is observed to be substantially smaller than that obtained with nonsymmetric 3D-BDML for $\Delta\Psi$ equal to 0°, 22.5°, 45°, 67.5°, and 180°.

The simulation results presented in Fig. 3 indicate that symmetric 3D-BDML significantly outperforms nonsymmetric 3D-BDML for most values of $\Delta\Psi$. This may be attributed to the use of a priori information by symmetric 3D-BDML with regard to the bisector angle. An indication of the sensitivity of symmetric 3D-BDML to error in the estimated bisector angle may be gleaned from observing the simulation results plotted in Fig. 4. For a given test case, the error cited

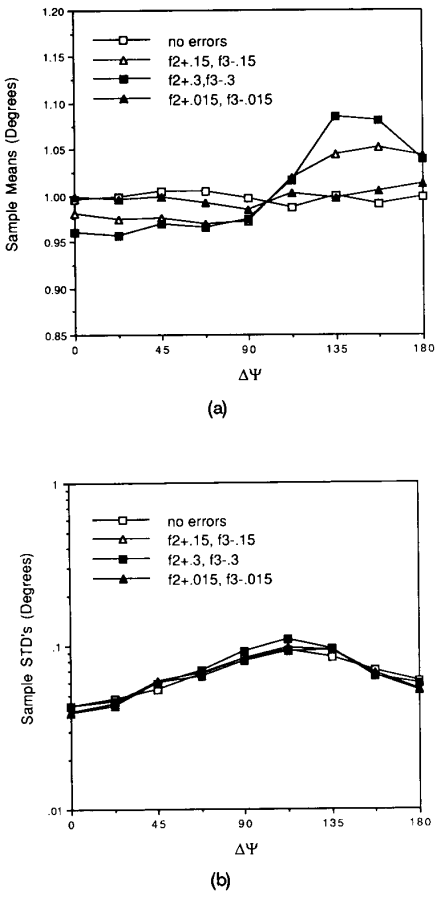

Fig. 7. Sensitivity of Symmetric 3D-BDML in case of multifrequency operation to deviations (in GHz) from the prescription $f_i = (M/M_i)f_0$, $i = 2,3$, where $f_0 = 10$ GHz, $M_2 = 19$ and $M_3 = 17$, for the two auxiliary frequencies employed in the simulations presented in Fig. 6. Simulation parameters are same as those described in caption to Fig. 6. (a) Direct path sample means. (b) Direct path sample STDs.

in the legend is defined as $\theta_B - \theta_c$, where θ_c is the pointing angle of the center beam and θ_B is the actual bisector angle equal to $-0.25°$ in this example. The performance statistics plotted for the no-error case are exactly the same as those associated with the symmetric 3D-BDML estimator plotted in Fig. 3. (Note the change in scale, however, between the vertical axes in Figs. 3(a) and 4(a), respectively.) For the error levels tested, which in view of the result in (5) correspond to fairly gross errors, very little difference is observed among the respective sample STD curves. On the other hand, an examination of the respective sample mean curves substantiates the conjecture made in Section III that the error in the bisector angle estimate translates into a bias in the symmetric 3D-BDML estimator of the same magnitude.

As an illustrative example, consider the case $\theta_c = -0.15°$, which corresponds to an error of $\theta_B - \theta_c = 0.1°$. In accordance with the discussion in Section III, the process of forward-backward averaging creates an artificial source at $2\theta_c - \theta_1 = 2(-0.15°) - 1° = -1.3°$ and another at $2\theta_c - \theta_2 = 2(-0.15°) - (-1.5°) = 1.2°$. Symmetric 3D-BDML cannot resolve the actual source at 1° and the artificial source at 1.2°, as they are angularly separated by 0.036 beamwidths, and in light of the nearly equal strength among the two sources, "sees" a single source at $\frac{1}{2}\{1° + 1.2°\} = 1.1°$. Correspondingly, we observe that with an error in the bisector angle of 0.1°, the sample mean obtained with symmetric 3D-BDML estimator of the direct path angle is 1.1° for most of the nine phase values tested.

The sample mean curves in Fig. 4(a) also suggest that an error in the bisector angle estimate pejoratively effects performance rather substantially in the case of $\Delta\Psi = 180°$. However, it should again be noted that the error levels tested represented gross deviations. In addition, the use of frequency diversity should remedy this problem.

The next set of simulation results examine the effect of removing the specular multipath component from the data, corresponding to $\rho = 0$. As discussed in Section III, the process of forward-backward averaging in the execution of symmetric 3D-BDML nevertheless creates an artificial source at $2\theta_c - \theta_1$, where θ_c is the pointing angle of the center beam. Thus, despite the absence of specular multipath, symmetric 3D-BDML must nevertheless resolve two sources separated by $2(\theta_c - \theta_1)$. Hence, the closer θ_c is to θ_1, the "harder" symmetric 3D-BDML must work to resolve the actual source and the artificial source. This translates into an increase in the sample STD of the bearing estimates as the separation between θ_1 and θ_c decreases, as illustrated in Fig. 5(b). For purposes of comparison, the sample means and sample STDs achieved with 2D-BDML for the same set of parameters are plotted in Figs. 5(a) and 5(b), respectively, as well. The absence of a specular multipath component renders 2D-BDML a viable bearing estimation procedure. With 2D-BDML, resolution is not an issue and, as a consequence, the sample STD does not vary much with respect to the location of the pointing angles of the two beams employed. Also, as expected, the sample STDs achieved with 2D-BDML are significantly lower than the respective sample STDs achieved with symmetric 3D-BDML for each of the different beam locations tested.

The simulation results presented in Fig. 6 compare the performance of nonsymmetric 3D-BDML with that of symmetric 3D-BDML employing the true bisector angle in the case of multifrequency operation. $J = 3$ frequencies satisfying $f_j M_j$ = constant were employed with $f_1 = f_0$ and $M_1 = M$. This corresponds to no spatial smoothing and, hence, use of the full aperture at f_0. In turn, this automatically dictates that the other two frequencies satisfy $f_j M_j = f_1 M_1 = 21 f_0$, or $f_j = (21/M_j)f_0$, $j = 2,3$, where M_j is an integer strictly

less than 21. The specific selections were $M_2 = 19$ and $M_3 = 17$ yielding the frequencies $f_2 = \frac{21}{19} f_0 = 1.105 f_0$ and $f_3 = \frac{21}{17} f_0 = 1.235 f_0$. Let $\Delta\Psi_i$, $i = 1,2,3$, denote the phase difference occurring at the center element, modulo 360°, at the respective frequency f_i, $i = 1,2,3$. Further, let $\Delta\Psi_{0,T}$ denote the total phase difference between the direct and specular path signals at the center element at $f_1 = f_0$ counting integer number of wavelengths delays, i.e., without the modulo by 360° operation. The values of $\Delta\Psi_i$, $i = 1,2,3$, were determined from $\Delta\Psi_{0,T}$ according to

$$\Delta\Psi_i = \left\{ \frac{f_i}{f_0} \{\Delta\Psi_{0,T} - 180°\} + 180°, \text{mod}(360°) \right\} \qquad i = 1,2,3 \qquad (58)$$

in accordance with the low-angle radar model described by Skolnik [19]. Note that this formula accounts for a 180° phase shift occurring at the surface of reflection. The phase shift occurring at the point of reflection is a phenomenon discussed by Skolnik [19] and Barton [1]. Note that in Fig. 6 (and Fig. 7 as well), $\Delta\Psi_1$ is simply denoted $\Delta\Psi$.

The performance statistics plotted in Figs. 6(a) and 6(b) demonstrate the robustness to the phase difference at any one frequency achieved with multifrequency operation. Although this is true for both nonsymmetric 3D-BDML and symmetric 3D-BDML, it is observed that the sample STDs achieved with symmetric 3D-BDML are smaller than the respective sample STDs achieved with nonsymmetric 3D-BDML for all nine values of $\Delta\Psi_1 = \Delta\Psi$ tested, with the differential between the two quite substantial for values of $\Delta\Psi$ near zero. It is noted that in all cases the sample bias achieved with symmetric 3D-BDML is less than 0.015° and the corresponding SSTD is less than 0.07°.

To emphasize the computational simplicity of symmetric 3D-BDML with multiple frequencies satisfying $f_j M_j$ = constant, we summarize the specific form of the algorithm employed in the simulations presented in Fig. 6. Recall that $f_1 = f_0$ and $M_1 = M$. $S_{M_2}(f_2)$, with $f_2 = \frac{21}{19} f_0$ and $M_2 = 19$, is applied to each of two overlapping subarrays of 19 contiguous elements and $\tilde{\mathbf{R}}_{bb}(f_2)$ is formed as the arithmetic mean of the outer products of the two 3×1 beamspace snapshot vectors thus created. Similar processing occurs at $f_3 = \frac{21}{17} f_0$ with $M_3 = 17$ to create $\tilde{\mathbf{R}}_{bb}(f_3)$. With $\overline{\mathbf{R}}_{bb} = \frac{1}{3} \sum_{j=1}^{3} \tilde{\mathbf{R}}_{bb}(f_j)$, $\overline{\mathbf{R}}_{bb}^{fb}$ is formed as $\overline{\mathbf{R}}_{bb}^{fb} = \frac{1}{2}\{\overline{\mathbf{R}}_{bb} + \tilde{\mathbf{I}}_3 \overline{\mathbf{R}}_{bb} \tilde{\mathbf{I}}_3\}$. $\mathbf{v} = [v_1, v_2, v_1]^T$ is then computed as that centro-symmetric eigenvector of $\text{Re}\{\overline{\mathbf{R}}_{bb}\}$ associated with the smaller eigenvalue. Finally, $\hat{u}_1$ is computed according to (32) since $f_1 = f_0$ and $M_1 = M$.

In a real-world application, the actual value of a transmission frequency will only match the desired value to within a certain tolerance. For example, in the MARS system described previously, the smallest increment the frequency of the agile transmitter may be stepped is 30 MHz. Suppose that specific values of f_1 and M_1 are selected, say $f_1 = f_0 = 10$ GHz and $M_1 = M = 21$, for example. Further, in determining two auxiliary frequencies to satisfy $f_j M_j$ = constant, we select $M_2 = 19$ and $M_3 = 17$ as above, such that $f_2 = \frac{21}{19} f_0 = 11.05$ GHz and $f_3 = \frac{21}{17} f_0 = 12.35$ GHz. These frequencies are in the range of the agile transmitter in the MARS system. The best we can do is synthesize these frequencies to within a tolerance of ±15 MHz = ±.015 GHz. For the sake of illustration, consider that instead of $f_2 = 11.05$ GHz and $f_3 = 12.35$ GHz, the actual transmission frequencies are $f_2' = f_2 + 0.015 = 11.065$ GHz and $f_3' = f_3 - 0.015 = 12.335$ GHz. And, despite the fact that $f_j' M_j \neq 21 f_0$, $j = 2,3$, we nevertheless employ the simplified multifrequency version of symmetric 3D-BDML outlined above. The resulting performance is plotted in Fig. 7 and compared with the performance achieved with f_2 and f_3 equal to the desired values of 11.05 GHz and 12.35 GHz, respectively, signified by the "no errors" label in the legend. The difference between the respective sample mean curves is practically negligible, as is the difference between the respective sample STD curves.

To really demonstrate the robustness of the method, the magnitude of the respective error in the two auxiliary frequencies was increased by a factor of ten, to 150 MHz, yielding the actual transmission frequencies $f_2' = f_2 + 0.15 = 11.2$ GHz and $f_3' = f_3 - 0.15 = 12.2$ GHz. Again, very little difference between the respective sample STD curves is observed. However, the corresponding sample mean curve does reveal a phase dependent bias: the sample bias is negative for values of $\Delta\Psi$ less than or equal to 90° and positive for values of $\Delta\Psi$ greater than 90°. A phase dependent sample bias curve of similar shape is obtained if the magnitude of the respective error in the two auxiliary frequencies is further increased by a factor of two, to 300 MHz, yielding the actual transmission frequencies $f_2' = f_2 + 0.3 = 11.35$ GHz and $f_3' = f_3 - 0.3 = 12.05$ GHz. As might be expected, the maximum sample bias obtained with these frequencies is about twice that obtained with $f_2' = f_2 + 0.15 = 11.2$ GHz and $f_3' = f_3 - 0.15 = 12.2$ GHz.

VI. CONCLUSIONS

3D-BDML is a computationally simple ML bearing estimation algorithm for low-angle radar tracking which operates in a 3-D beamspace generated by three orthogonal, classical beamformers with equi-spaced pointing angles. In symmetric 3D-BDML the pointing angle of the center beam is equal to the bisector angle between the direct path ray and the image ray, yielding a 1-D parameter estimation problem. The bisector angle may be accurately estimated a *priori* given the height of the receiving array and

an estimate of the range of the target. In contrast, nonsymmetric 3D-BDML does not account for the multipath geometry and effectively solves a 2-D parameter estimation problem. As a consequence, we find that that nonsymmetric 3D-BDML breaks down when $\Delta\Psi$, the phase difference between the direct and specular path signals at the aperture center, is either 0° or 180°. In contrast, symmetric 3D-BDML can theoretically handle any value of $\Delta\Psi$ with $\Delta\Psi = 0°$ yielding best performance.

In terms of processing, the only difference between symmetric 3D-BDML and nonsymmetric 3D-BDML is the forward-backward averaging of the 3×3 beamspace correlation matrix performed in symmetric 3D-BDML. If the pointing angle of the center beam is not equal to the bisector angle, the process of forward-backward averaging serves to effectively create artificial sources at the mirror images of the actual sources about the pointing angle of the center beam. A simple analysis of this phenomenon reveals that an error in the bisector angle estimate translates into a bias in the symmetric 3D-BDML estimator of the same magnitude. In the case of no specular multipath, this phenomenon makes the symmetric 3D-BDML estimator nevertheless have to resolve two sources separated by less than a beamwidth. The 2D-BDML estimator may be used under these conditions to achieve better performance.

Although symmetric 3D-BDML is theoretically capable of handling any value of $\Delta\Psi$, performance in the case of $\Delta\Psi = 180°$ is rather poor. An obvious means for overcoming this problem is to employ frequency diversity. It has been shown that if the transmission frequencies satisfy $f_j M_j = \text{constant}$, $j = 1,\ldots,J$, where $M_j \leq M$ is the number of elements comprising the subarray employed at f_j, coherent signal subspace averaging is achieved by simply summing the (spatially smoothed) beamspace correlation matrices formed at each frequency. The multifrequency version of symmetric 3D-BDML is then simply the single frequency version executed with the coherently averaged beamspace correlation matrix thus obtained. Simulations demonstrating the method to be rather robust to relatively large deviations in the product $f_j M_j$ from frequency to frequency suggest that the procedure may indeed be practicable.

ACKNOWLEDGMENT

The authors gratefully acknowledge valuable criticisms and practical comments made by an anonymous reviewer with regard to incorporating the multipath geometry as a priori information. This reviewer supplied Table I and is the source of the procedure for estimating the bisector angle in the case of a spherical Earth model described in Section II.

REFERENCES

[1] Barton, D. K. (1974)
Low angle radar tracking.
Proceedings of the IEEE, **62** (June 1974), 687–704.

[2] Ksienski, A. A., and McGhee, R. B., Jr. (1968)
A decision theoretic approach to the angular resolution and parameter estimation problem for multiple targets.
IEEE Transactions on Aerospace and Electronic Systems, **AES-4** (May 1968), 443–445.

[3] White, W. D. (1974)
Low-angle radar tracking in the presence of multipath.
IEEE Transactions on Aerospace and Electronic Systems, **AES-10** (Nov. 1974), 835–853.

[4] Gabriel, W. F. (1984)
A high-resolution target-tracking concept using spectral techniques.
Report 6109, Naval Research Laboratory, Washington, DC, May 1984.

[5] Davis, R. C., Brennan, L. E., and Reed, L. S. (1976)
Angle estimation with adaptive arrays in external noise fields.
IEEE Transactions on Aerospace and Electronic Systems, **AES-12**, 3 (Mar. 1976), 179–186.

[6] Cantrell, B. H., Gordon, W. B., and Trunk, G. V. (1981)
Maximum likelihood elevation angle estimation of radar targets using subapertures.
IEEE Transactions on Aerospace and Electronic Systems, **AES-17**, 3 (Mar. 1981), 213–221.

[7] Kesler, J., and Haykin, S. (1980)
A new adaptive antenna for elevation angle estimation in the presence of multipath.
IEEE 1980 Antenna and Propagation International Symposium Digest (June 1980), 130–133.

[8] Haykin, S. (1985)
Radar array processing for angle of arrival estimation.
In *Array Signal Processing*. Englewood Cliffs, NJ: Prentice-Hall, 1985, ch. 4.

[9] Gordon, W. B. (1983)
Improved three subaperture method for elevation angle estimation.
IEEE Transactions on Aerospace and Electronic Systems, **AES-19**, 1 (Jan. 1983), 114–122.

[10] Ballance, W. P., and Jaffer, A. G. (1987)
Low angle direction finding based on maximum likelihood: A unification.
Conference Record of the 21st Asilomar Conference on Signals, Systems, and Computers, (Nov. 1987), 119–124.

[11] Zoltowski, M. (1988)
High resolution sensor array signal processing in the beamspace domain: Novel techniques based on the poor resolution of Fourier beamforming.
In *Proceedings of the Fourth ASSP Workshop on Spectrum Estimation and Modeling*, (Aug. 1988), 350–355.

[12] Lee, T. S., and Zoltowski, M. (1989)
Beamspace domain ML based low angle radar tracking with an array of antennas.
IEEE Antennas and Propagation Symposium Digest, San Jose, CA, June 1989.

[13] Zoltowski, M., and Lee, T. S. (1991)
Maximum likelihood based sensor array signal processing in the beamspace domain for low-angle radar tracking.
In *IEEE Transactions on Acoustics, Speech, and Signal Processing*, **ASSP-39**, 3 (Mar. 1991), 656–671.

[14] Gabriel, W. F. (1988)
Large-aperture sparse array antenna systems of moderate bandwidth for multiple emitter location.
In *Proceedings of the Fourth Workshop on Spectrum Estimation and Modeling*, (Aug. 1988), 7–12.

[15] Shan, T. J., Wax, M., and Kailath, T. (1985)
On spatial smoothing for direction-of-arrival estimation of coherent signals.
IEEE Transactions on Acoustics, Speech, and Signal Processing, **33** (Aug. 1985), 806–811.

[16] Williams, R. T., Prasad, S., Mahalanabis, A. K., and Sibul, L. H. (1988)
An improved spatial smoothing technique for bearing estimation in a multipath environment.
IEEE Transactions on Acoustics, Speech, and Signal Processing, **36** (Apr. 1988), 425–432.

[17] Schmidt, R. (1979)
Multiple emitter location and signal parameter estimation.
In *Proceedings of the RADC Spectral Estimation Workshop*, Rome, NY, 1979, 243–256.

[18] Kezys, V., and Haykin, S. (1988)
Multifrequency angle-of-arrival estimation: An experimental evaluation.
In *Proceedings of the SPIE Int'l. Symposium, Advanced Algorithms and Architectures for Signal Processing III*, **975** (Aug. 1988), 98–106.

[19] Skolnik, M. I. (1980)
Introduction to Radar Systems.
New York: McGraw-Hill, 1980, 442–446.

[20] Wang, H., and Kaveh, M. (1985)
Coherent single-subspace averaging for the detection and estimation of angles of arrival of multiple wide-band sources.
IEEE Transactions on Acoustics, Speech, Signal Processing, **ASSP-33**, 4 (Aug. 1985), 823–831.

[21] Hung, H., and Kaveh, M. (1988)
Focusing matrices for coherent single-subspace processing.
IEEE Transactions on Acoustics, Speech, Signal Processing, **ASSP-36**, 8 (Aug. 1988), 1272–1281.

[22] Lee, T. S. (1989)
Beamspace domain ML based low-angle radar tracking with an array of antennas.
Ph.D. dissertation, Purdue University, Dec. 1989.

Michael D. Zoltowski (S'79—M'86) was born in Philadelphia, PA on August 12, 1960. He received the B.S. and M.S. degrees in electrical engineering with highest honors from Drexel University, Philadelphia, in 1983 and his Ph.D. in systems engineering from the University of Pennsylvania, Philadelphia, in 1986.

From 1982 to 1986, he was an Office of Naval Research Graduate Fellow. In conjunction with his Fellowship, he held a visiting research position at the Naval Research Laboratory in Washington, DC, during Summer 1986. In Fall 1986, he joined the faculty of Purdue University where he currently holds a position of Assistant Professor of Electrical Engineering. During 1987, he held a position of Summer Faculty Research Fellow at the Naval Ocean Systems Center in San Diego, CA. His present research interests include sensor array signal processing, phased array radar, sonar, adaptive signal processing, higher order spectral analysis, and numerical linear algebra. He presently serves as a consultant to the General Electric Company.

Dr. Zoltowski is a member of Eta Kappa Nu, Tau Beta Pi, Phi Eta Sigma, and Phi Kappa Phi.

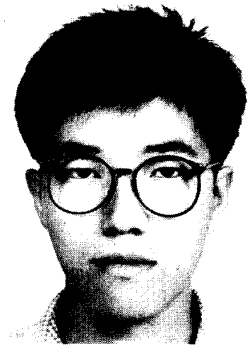

Ta-Sung Lee (S'88) was born in Taipei, Taiwan, Republic of China on October 20, 1960. He received the B.S. degree from National Taiwan University, in 1983, the M.S. degree from University of Wisconsin at Madison in 1987, and the Ph.D. degree from Purdue University, West Lafayette, IN, in 1989, all in electrical engineering.

From 1987 to 1989, he was a David Ross Graduate Research Fellow at Purdue University. In Spring 1990, he joined the faculty of National Chiao Tung University, Hsinchu, Taiwan, where he currently holds a position of Associate Professor in the Department of Communication Engineering. His research interests include sensor array signal processing, bandlimited signal analysis, and adaptive equalization.